Inorganic Chemistry

pubs.acs.org/IC Article

Evidence for Uranium(VI/V) Redox Supported by 2,2′-Bipyridyl-6,6′-dicarboxylate

Emily R. Mikeska, Alexander C. Ervin, Kaihua Zhang, Gabriel M. Benitez, Samuel M. R. Powell, Allen G. Oliver, Victor W. Day, Marco Caricato,* Chelsea G. Comadoll,* and James D. Blakemore*

Cite This: *Inorg. Chem.* 2023, 62, 16131−16148 Read Online

ACCESS | Metrics & More | Article Recommendations | Supporting Information

ABSTRACT: The 2,2′-bipyridyl-6,6′-dicarboxylate ligand (**bdc**) has been shown in prior work to effectively capture the uranyl(VI) ion, UO_2^{2+}, from aqueous solutions. However, the redox properties of the uranyl complex of this ligand have not been addressed despite the relevance of uranium-centered reduction to the nuclear fuel cycle and the presence of a bipyridyl core in **bdc**, a motif long recognized for its ability to support redox chemistry. Here, the **bdc** complex of UO_2^{2+} (**1-UO$_2$**) has been synthetically prepared and isolated under nonaqueous conditions for the study of its reductive chemical and electrochemical behavior. Spectrochemical titration data collected using decamethylcobaltocene (Cp^*_2Co) as the reductant demonstrate that $1e^-$ reduction of **1-UO$_2$** is accessible, and companion near-infrared and infrared spectroscopic data, along with theoretical findings from density functional theory, provide evidence that supports the accessibility of the U(V) oxidation state. Data obtained for control ruthenium complexes of **bdc** and related polypyridyl dicarboxylate ligands provide a counterpoint to these findings; ligand-centered reduction of **bdc** in these control compounds occurs at potentials more negative than those measured for reduction of **1-UO$_2$**, further supporting the generation of uranium(V) in **1-UO$_2$**. Taken together, these results underscore the usefulness of **bdc** as a ligand for actinyl ions and suggest that it could be useful for further studies of the reductive activation of these unique species.

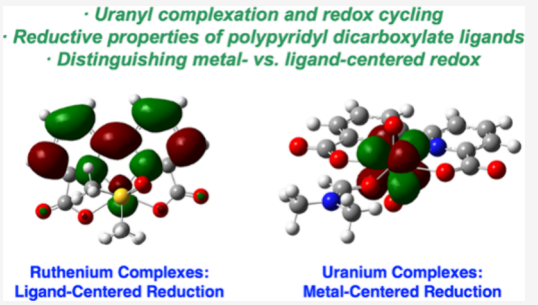

INTRODUCTION

Changing the formal oxidation state of actinide-containing complexes has been established as an important method for directly influencing solubility, reactivity, and speciation properties.[1] In nuclear fuel reprocessing chemistry, redox-driven swings in speciation have been used to achieve useful separations that can lower the total amount of waste associated with nuclear power production.[2] Similarly, redox chemistry governs the speciation of actinides such as uranium, neptunium, and plutonium in the environment, opening the opportunity for design of reagents and/or conditions that can sequester actinides and/or remediate contaminated areas.[3] Along the same lines, the development of tailored ligands that can effectively bind to actinides has enabled the study and control of the molecular redox properties of these important elements. In the case of uranium, the uranyl dication (UO_2^{2+}) dominates behaviors under most conditions, and thus, a considerable effort has been focused on this species.[4]

Significant work has focused on the question of the site of reduction and oxidation in molecular actinide complexes as electrons can be transferred to/from metal-centered orbitals, ligand-centered orbitals, or orbitals that span both metal and ligands.[5,6] Distinguishing between these different cases can be aided by electrochemical, spectroscopic, and theoretical techniques, each giving insight into the nature of the products arising from specific electron transfer events.[7] Fortier and coworkers specifically explored the question of the uranium oxidation state in the homoleptic 2,2′-bipyridyl (bpy) complex of uranium [$U(bpy)_4$], emphasizing the importance of consideration of metal- vs ligand-centered redox in complexes containing ligands that display π-conjugation in particular.[8] Assignment of the nature of the accessible redox events in systems is valuable, as the site of the gain or loss of electrons from metals or ligands in many cases dictates observed reactivity patterns. This is certainly the case for the uranium(V) oxidation state of the uranyl ion,[9] which has been demonstrated to display increased Lewis basicity upon generation from UO_2^{2+},[10] leading to exciting developments in oxo functionalization chemistry,[11] stabilization of the uranium(V) oxidation state that is less commonly encountered,[12,13] and studies of further reduction of uranyl itself.[14]

Considering these opportunities, a portion of our attention has recently been drawn to the uranyl complex of the 2,2′-

Received: July 13, 2023
Published: September 18, 2023

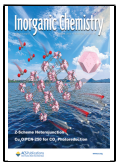

https://doi.org/10.1021/acs.inorgchem.3c02397
Inorg. Chem. 2023, 62, 16131−16148

Chart 1. Established Preparation of a Ru(II) Complex of 2,2′-Bipyridyl-6,6′-dicarboxylate Reported by Sun and Co-Workers in Comparison with the Reported In Situ Generation of a U(VI) Complex of 2,2′-Bipyridyl-6,6′-dicarboxylate

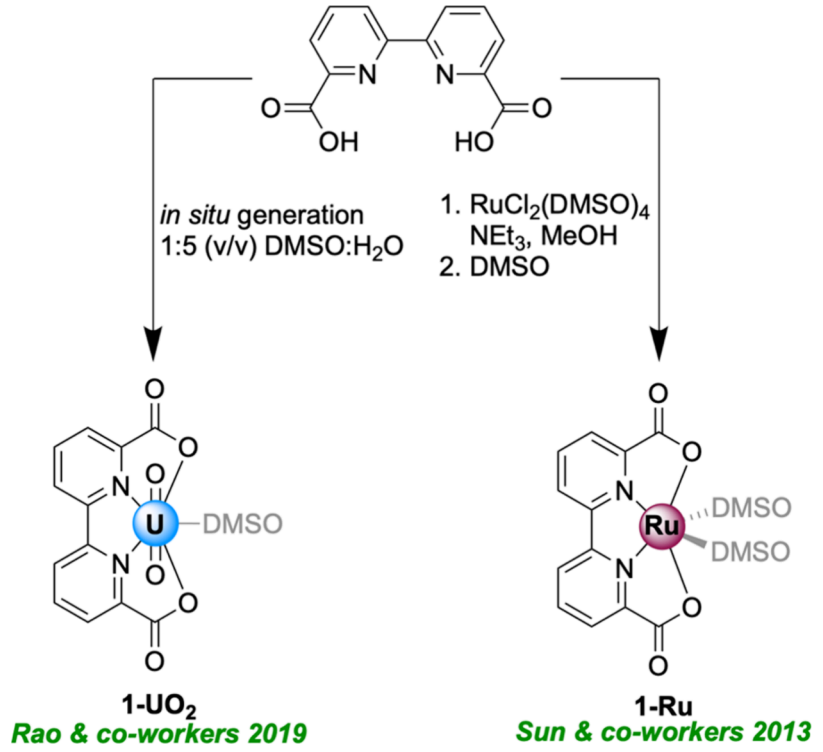

bipyridyl-6,6′-dicarboxylate ligand (**bdc**).[15,16] This complex has been reported previously to form spontaneously under aqueous conditions, suggesting that its high stability may derive from the tetradentate nature of **bdc** as a ligand. Additionally, as **bdc** features two proton-responsive carboxylate moieties, the ligand has an accessible dianionic form that can support an overall neutral complex of UO_2^{2+}. However, synthetic methods for conventional isolation and/or characterization of this complex have not been included in literature reports (see Chart 1).[15] We also note here that **bdc** is well-known outside of *f*-element chemistry for its robustness, as it has been used to support ruthenium-based molecular catalysts for water and ammonia oxidation.[17,18] Adding appeal for further development of **bdc** coordination chemistry, the ligand itself can be readily prepared on a large scale (4 g per batch in our hands) from commercially available 6,6′-dimethyl-2,2′-bipyridyl.[19,20] In light of all these features, we anticipated that an examination of the nonaqueous synthesis and redox chemistry of the **bdc** complex of uranyl could provide evidence for the accessibility of the uranium(V) oxidation state on this ligand platform, an attractive prospect since the uranium(VI) complex appears to form spontaneously under some conditions, as noted previously. From the perspective of ligand development, we also anticipated that electrochemically and spectroscopically addressing the previously unexplored redox activity of the 2,2′-bipyridyl core in the **bdc** ligand itself could further accelerate the use of this platform in specific applications.

Here, we report the nonaqueous synthesis and redox properties of **bdc**-ligated uranyl complexes. Synthetic investigations show that UO_2^{2+} is readily captured by **bdc** under nonaqueous conditions, enabling isolation of complexes of the form UO_2(bdc)L, where L = dimethylsulfoxide (**1-UO$_2$**) or triethylamine (**1-UO$_2$′**). Nuclear magnetic resonance data are in accordance with tetradentate coordination of the **bdc** core to the metal centers in both cases, a finding further supported by structural data from X-ray diffraction analysis. In line with the tetradentate nature of **bdc**, evidence shows that an exogenous, fifth ligand (here, solvent) binds to the uranium center in the complexes. Electronic absorption spectra of **1-UO$_2$** reveal the vibronic structure in a ligand-to-metal charge transfer transition within the uranyl unit of the complex; minor shifts in the transition energies of the vibronic features were measured in different solvents, suggesting that ligand exchange occurs under the chosen conditions. Spectrochemical titration data reveal that decamethylcobaltocene is sufficiently reducing to drive the 1e$^-$ reduction of **1-UO$_2$**, whereas cobaltocene is not sufficiently reducing; these findings are in accordance with electrochemical data, suggesting that the complex undergoes a first reduction near −1.35 V vs ferrocenium/ferrocene (denoted hereafter as $Fc^{+/0}$). Spectral data from the UV, visible, and most importantly, near-infrared regions support the assignment of this first reduction as metal-centered, giving rise to a detectable uranium(V) form of the compound in solution. Comparisons to control Ru(II) complexes underscore distinguishing features of metal- vs ligand-centered reduction events in complexes supported by **bdc** and its analogues. Computational findings from density functional theory (DFT) are in accordance with these results, suggesting that the uranium(VI) center in **1-UO$_2$** is the most likely site of reduction, whereas the control ruthenium complexes undergo ligand reduction in the 2,2′-bipyridyl core of **bdc**.

RESULTS

Synthesis of Uranyl Polypyridyl Dicarboxylate Complexes 1-UO$_2$ and 1-UO$_2$′. While **H$_2$bdc** has been explored as a complexing agent for UO_2^{2+} and the crystal structure of a **bdc**-complexed UO_2^{2+} species reported, the preparative

https://doi.org/10.1021/acs.inorgchem.3c02397
Inorg. Chem. 2023, 62, 16131−16148

chemistry of H_2**bdc** with UO_2^{2+} has not been investigated.[15] Therefore, we developed a synthetic route that affords the **bdc**-ligated UO_2^{2+} complex **1-UO$_2$** under nonaqueous conditions in order to facilitate studies on the tractability of uranium-based redox chemistry in this system. Our synthetic strategy under these nonaqueous conditions was based on prior methods used in our group for the handling of uranyl that rely on protonolysis reactivity.[12] We found that this approach is effective for this complex as well, such that stirring H_2**bdc** and uranyl acetate dihydrate in dimethylsulfoxide (DMSO) followed by the addition of excess diethyl ether results in the precipitation of **1-UO$_2$** cleanly from solution in good yields. The ^{1}H NMR spectrum of the resulting yellow powder in d_6-DMSO confirmed the presence of DMSO as a fifth equatorial ligand to uranyl; a unique resonance, shifted slightly downfield from the typical protio-residual signal for d_6-DMSO (referenced to 2.50 ppm[21]), was measured at 2.54 ppm, corresponding to the equivalent methyl protons of bound DMSO. This singlet integrates to 6H with respect to the individual protons measured for the **bdc** ligand core, as expected (see the SI, Figure S1).

In an effort to avoid the use of DMSO in the synthesis, we also developed a synthetic route to access a **bdc**-supported uranyl complex, in which methanol was used as the solvent. Under these conditions, 3 equiv of triethylamine was used as an auxiliary base to deprotonate the carboxylic acid groups of free H_2**bdc**. Concentration of the reaction mixture by the removal of solvent after refluxing overnight in the presence of uranyl acetate dihydrate, followed by washing of the material with ether, resulted in the isolation of a yellow solid, denoted as **1-UO$_2$′**. Similar to the case of **1-UO$_2$**, the ^{1}H NMR spectrum of **1-UO$_2$′** in d_4-MeOH confirmed the ligation of UO_2^{2+} by the tetradentate **bdc**, although in this case, the spectrum suggests that triethylamine (NEt_3) is present as the fifth equatorial ligand to uranyl. The bound NEt_3 moiety was observed as a quartet at 3.24 ppm and triplet at 1.32 ppm, signals that are, as expected, shifted downfield relative to those of free triethylamine at 2.58 and 1.05 ppm, respectively (see the SI, Figure S3).[21] These NMR data suggest that triethylamine remains bound to the uranium center in the presence of methanol as the solvent. Finally, elemental analysis data of **1-UO$_2$′** show that its formulation is consistent with UO_2^{2+} incorporation into the **bdc** framework with NEt_3 as the fifth equatorial ligand (see the Experimental Section).

Encouraged by our isolation of these uranyl complexes, we characterized each complex, the free ligand H_2**bdc**, and uranyl acetate dihydrate with solid-state infrared spectroscopy (see the SI, Figures S21−S26 and Table S1). Shifts in peaks corresponding to the polypyridyl dicarboxylate ligand backbones were observed and are consistent with the ligation of uranyl in both **1-UO$_2$** and **1-UO$_2$′**. Inspection of the fingerprint region of the spectra also revealed stretches that can be assigned as the asymmetric uranyl U−O vibrations at 908 cm^{-1} for **1-UO$_2$** and 912 cm^{-1} **1-UO$_2$′** as well as possible weak U−N stretches at 575 and 577 cm^{-1} for **1-UO$_2$** and **1-UO$_2$′**, respectively.[22] The asymmetric uranyl U−O vibrations of **1-UO$_2$** and **1-UO$_2$′** are shifted from that of the uranyl acetate dihydrate starting material for which the noted feature appears at 945 cm^{-1} (Figure S26). In each case, peaks consistent with the presence of DMSO or NEt_3 as the respective equatorial solvent ligands for **1-UO$_2$** and **1-UO$_2$′** were also detected as an ν(S−O) stretch in the spectrum of **1-UO$_2$** at 1082 cm^{-1} and an ν(C−N) stretch in the spectrum of **1-UO$_2$′** at 1271 cm^{-1} (see the SI, Figures S21 and S22). In both cases, shifts of the asymmetric uranyl stretch and the ligand stretches are consistent with the formation of polypyridyl dicarboxylate uranyl complexes, highlighting the ability of polypyridyl dicarboxylate ligands to form stable complexes of uranyl.

As described in the Introduction, a prime goal of this study was to distinguish between metal- vs ligand-centered redox processes in compounds supported by **bdc**. To accomplish this, we elected to prepare control compounds of ruthenium(II) with **bdc** and two related polypyridyl dicarboxylates that feature larger π systems, 2,2′:6′,2″-terpyridyl-6,6″-dicarboxylate (**tdc**) and 4′-phenyl-2,2′:6′,2″-terpyridyl-6,6″-dicarboxylate (^{Ph}**tdc**) to examine trends in the spectroscopic and structural data (see Chart 2).[23] In addition to its reliable coordination chemistry with **bdc**, ruthenium(II) was chosen for the fair solubility of its complexes as well as its documented inertness toward reduction, enabling isolation in our investigation of ligand-based redox processes in the control complexes.[24,25] We also note here that we were inspired to pursue the ruthenium control compounds because the synthetic chemistry of the desired species appeared quite tractable in comparison with, for example, the synthesis of analogous zinc complexes. Zinc, in the form of Zn(II) salts, has often been used to prepare model species for the study of ligand-centered reduction processes in light of the negative standard reduction potential for the Zn^{II}/Zn^0 couple ($E°$ = −0.76 V).[26] In prior work, we showed that $[Zn(NCMe)_6]^{2+}$ undergoes reduction at a rather negative potential in acetonitrile ($E_{p,c}$ = −1.46 V),[27] a finding that could have motivated its use here to prepare the control complexes. However, to the best of our knowledge, there is only one prior report[28] of a molecular zinc complex of **bdc**; at the outset of this project, we did attempt some preliminary syntheses that targeted zinc(II) complexes, but these attempts yielded only intractable, insoluble materials in each case. Therefore, we chose to pursue the better precedented ruthenium species of **bdc**, **tdc**, and ^{Ph}**tdc** as spectroscopic/electrochemical control complexes, and the results from our studies of these compounds are included here.

Chart 2. Control Ruthenium Complexes Described in this Study[a]

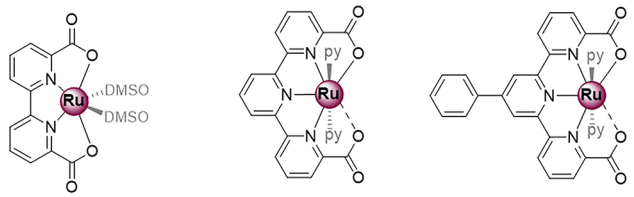

[a]Ruthenium is in the +2 formal oxidation state in all cases. The dashed lines represent long interatomic contacts observed in single-crystal X-ray diffraction analysis.

Synthesis of the desired complexes **1-Ru**, **2-Ru**, and **3-Ru** was achieved under conditions similar to those reported by Llobet and co-workers, and our ^{1}H NMR data of **1-Ru** and **2-Ru** matched those reported previously by Sun and Llobet (see SI, Figures S11 and S12).[29,30] For the newly reported complex **3-Ru**, ^{1}H and ^{13}C{^{1}H} NMR with related 2D NMR studies were used to confirm the formation of the desired complex,

https://doi.org/10.1021/acs.inorgchem.3c02397
Inorg. Chem. 2023, 62, 16131−16148

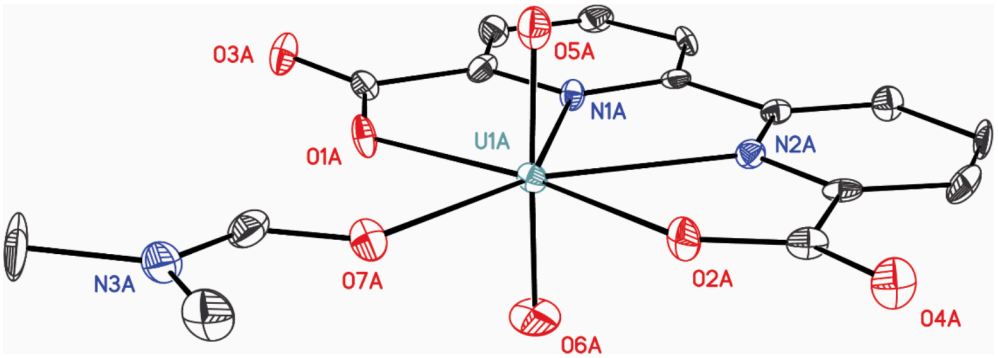

Figure 1. Solid-state structure (XRD) of **1-UO$_2$′**. All hydrogen atoms, a cocrystallized dimethylformamide molecule, and a second molecule of **1-UO$_2$′** found in the asymmetric unit are omitted for clarity. Displacement ellipsoids are shown at the 50% probability level.

which bears a high similarity to **2-Ru** (see the SI, Figures S13–S18). On the basis of both literature data and our characterizations, **bdc** and the related **tdc** and ^{Ph}**tdc** ligands adopt a tetradentate coordination to Ru(II); each of the complexes feature virtually octahedral Ru(II) centers.[17,30] Infrared spectra of **1-Ru**, **2-Ru**, and **3-Ru** in both the solid and solution phases display peaks corresponding to the functional groups present in the polypyridyl dicarboxylate ligand backbones of each complex (see the SI, Figures S32–S38).

Solid-State Structure of 1-UO$_2$′. In the prior study from Rao and co-workers, crystals of a **bdc**-ligated uranyl complex were grown in 1:5 (v/v) DMSO:H_2O from the in situ complexation of uranyl by **bdc**.[15] With this in mind, we investigated whether crystals could be grown of the isolated **1-UO$_2$′** material from a purely organic solvent system. We were also interested in comparing the structural parameters for **1-UO$_2$′** with those of the prior uranyl-**bdc** structure and the perhaps more broadly recognized Ru-**bdc** structure. Indeed, we found that crystals suitable for single-crystal XRD analysis of **1-UO$_2$′** could be grown by vapor diffusion of diethyl ether into a concentrated solution of **1-UO$_2$′** in N,N-dimethylformamide (DMF); the structure is reported in Figure 1. The presence of the coordinating solvent DMF in the crystallization environment led to the exchange of NEt_3 on **1-UO$_2$′** for DMF, bound to uranium through oxygen in the structure obtained (see the SI, pp. S75–S76 for details on this structure). In spite of the noted ligand exchange, most parameters for the prior structure of **1-UO$_2$** and our new structure are similar; the **bdc** ligand is bound to the uranyl ion in a κ^4-[N_2,O_2] fashion in both cases. The bpy core of **bdc** is quite planar when bound to uranyl, as it is in the case of **1-Ru**; we quantified this through measurement of the average torsion angle between the pyridyl rings in the bipyridyl ligand core (denoted as $\Theta_{inter\text{-}ring}$ in Table 1; the value of this parameter is a modest 3.5(1)° for **1-UO$_2$′**). Additionally, the oxo groups of the uranyl remain intact with U–O_{oxo} distances consistent with uranium in the +6 oxidation state (1.781(6) and 1.757(6) Å).[31]

In the structure of **1-UO$_2$′** (See the SI, pp. S75–S76 and Table S17), typical bond lengths and angles were observed that are in agreement with the previously reported structure of **1-UO$_2$**. In both **1-UO$_2$** and **1-UO$_2$′**, the uranium center sits more in-plane with the **bdc** ligand compared to the analogous Ru(II) complex **Ru(bdc)Me-py$_2$**, as quantified by the parameter Ψ_M in Table 1. Inspection of the M–ligand bond distances in the U(VI) and the Ru(II) complexes reveals longer U–ligand bonds than the analogous Ru–ligand bonds, consistent with the anticipated larger ionic radius of the uranium center. The bite angle of the bipyridyl core on the metal center is notably smaller for the uranium center in **1-UO$_2$′** than that in the case of the Ru center in **Ru(bdc)Me-py$_2$**; this is consistent with the positioning of the U center at a greater distance from the bpy core as well as the relatively rigid nature of the ligand backbone. Taking all of these trends and the metrical parameters together, these structures underscore the versatility of **bdc** to support both Ru(II) and U(VI) in a tetradentate fashion.

Table 1. Comparison of Selected Structural Parameters from X-ray Diffraction Analyses of 1-UO$_2$′, 1-UO$_2$, and Ru(bdc)Me-py$_2$

	1-UO$_2$′	1-UO$_2$	Ru(bdc)Me-py$_2$
Z	2	1	1
chelate coordination mode	κ^4-[N_2,O_2]	κ^4-[N_2,O_2]	κ^4-[N_2,O_2]
U–$O5_{oxo}$	1.781(6)[a]	1.78(1)	
U–$O6_{oxo}$	1.757(6)[a]	1.77(1)	
M–$N1_{average}$ (Å)	2.534(6)[a]	2.54(1)	1.914(7)
M–$N2_{average}$ (Å)	2.536(6)[a]	2.54(1)	1.950(8)
M–$O1_{average}$ (Å)	2.317(6)[a]	2.31(1)	2.216(7)
M–$O2_{average}$ (Å)	2.317(6)[a]	2.33(1)	2.172(7)
∠N1–M–N2	62.2(2)[a]	62.5(4)	81.2(3)
Ψ_M (Å)[b]	0.007	0.007	0.025
$\Theta_{inter\text{-}ring}$ (deg)[c]	3.5(1)[a]	2.0(2)	2.5(1)
reference	this work	ref 15	ref 24

[a]Value in parentheses refers to the e.s.d. that is the largest for an individual entry among the independent values used to compute the average. [b]Defined as the absolute value of the average distance between the metal atom and the mean plane defined by O1, N1, N2, and O2. [c]Defined as the absolute value of the average torsion angle between the pyridyl rings in the bipyridyl ligand cores.

Electronic Absorption Spectra. Having established the formulation of our materials isolated from synthesis under nonaqueous conditions, we next measured the electronic absorption properties of our complexes in DMF. In the case of **1-UO$_2$**, we measured strong absorption features between 265 and 340 nm which we ascribe to π-to-π^* transitions of the 2,2′-bipyridyl core on the basis of their large molar absorptivity values of approximately 10,500 M^{-1} cm^{-1} and resemblance to those of related complexes containing 2,2′-bipyridyl (see SI, Figures S39 and S40).[32,33] Additionally, we observed a rich feature with vibronic structure that can be assigned as arising from the uranyl unit itself; this feature can sometimes be measured for U(VI) complexes between 345 and 555 nm, although it is often obscured by lower energy ligand-to-metal

https://doi.org/10.1021/acs.inorgchem.3c02397
Inorg. Chem. 2023, 62, 16131–16148

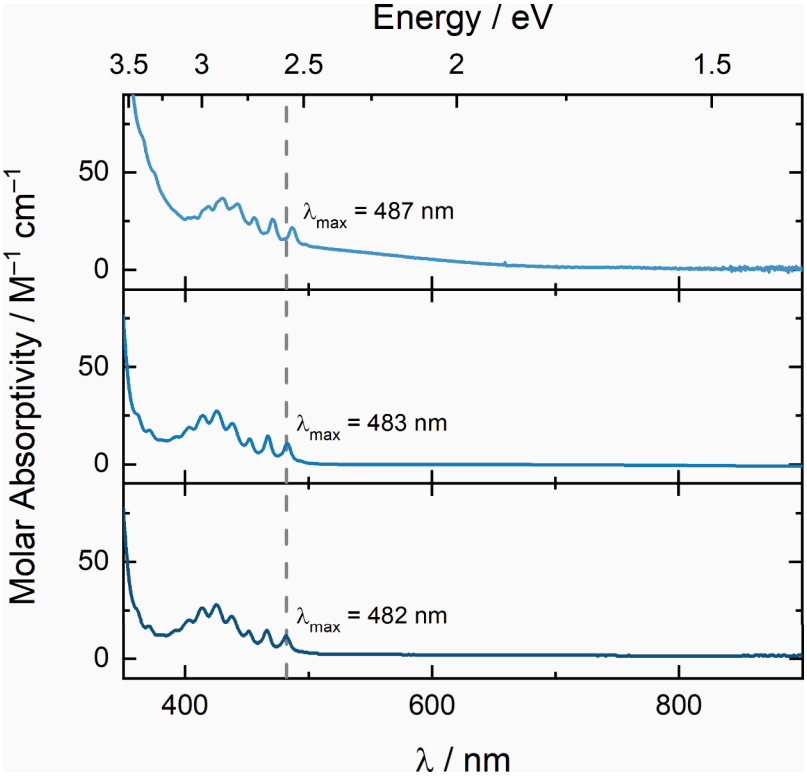

Figure 2. Electronic absorption spectra of **1-UO$_2$** in DMF (top), DMSO (middle), and a 1:5 (v/v) DMSO−H_2O mixture.

charge transfer (LMCT) bands involving equatorial ligands.[34,35] These features are most often observed in absorption spectra of simple salts of U(VI) or when the equatorial ligands surrounding uranyl are not strongly absorbing in this region.[36−38] Documented in a variety of media, this region typically reveals between 6 and 14 peak maxima with $\varepsilon \leq 100$ M^{-1} cm^{-1} due to LMCT transitions from the *-yl* oxygens of the uranyl unit into empty orbitals on U(VI).[39−41] Gratifyingly, we were able to observe these uranyl-based vibronic features in the spectra of **1-UO$_2$** as the absorptions based on the 2,2′-bipyridyl core appear at higher energies under our chosen measurement conditions.

With this appealing opportunity to probe these transitions of uranyl in organic solvents and in the presence of the tetradentate **bdc** ligand, we investigated variations in these transitions in the solvents DMF, DMSO, and a 1:5 (v/v) DMSO:H_2O mixture, where **1-UO$_2$** is highly soluble. In each solvent, seven peak maxima were clearly observed that exhibited the low molar absorptivity values expected for uranyl-based LMCT transitions ($\varepsilon_{430\ nm} \approx 36$ M^{-1} cm^{-1}), with additional shoulders distinguishable in spectra taken in DMSO and the 1:5 (v/v) DMSO:H_2O mixture (see Figure 2 and Figures S41 and S42 in the SI). Slight variations in the peak energies can be seen for **1-UO$_2$** in the various solvents, with **1-UO$_2$** in DMF displaying the most red-shifted feature at the lowest energy (2.55 eV) and **1-UO$_2$** in the DMSO:H_2O mixture showing the most red-shifted feature at the highest energy (2.57 eV; see Figure 2). As a result of the highly coordinating nature of the solvents used here and the inclusion of a DMSO solvent molecule in **1-UO$_2$** itself, we hypothesize that the differences in the peak energies of the features in the various solvents can be ascribed to solvent exchange in the equatorial belt of the U(VI) center. This is consistent with the solvent exchange observed during the crystallization of **1-UO$_2$**′ (vide supra) and the known propensity for solvent ligands to undergo rapid exchange at U(VI) centers.[42,43]

In the cases of the control ruthenium compounds, we also measured a strong absorption feature attributable to π-to-π^* transitions of the 2,2′-bipyridyl core at λ_{max} = 302 nm for **1-Ru** (see the SI, Figures S56 and S57).[32,33] The spectrum of **1-Ru** also contains two broad absorptions attributable to metal-to-ligand charge transfer (MLCT) bands between 320 and 520 nm, which are in agreement with the expected bands for ruthenium in the +2 oxidation state.[30] Similar profiles were also observed for **2-Ru** and **3-Ru** showing both the strongly absorbing features in the UV region (λ_{max} = 280 and 333 nm for **2-Ru**, λ_{max} = 292 and 338 nm for **3-Ru**; see the SI, Figures S58 and S61) as well as the two broad absorptions in the visible region (λ_{max} = 498 and 548 nm for **2-Ru**, λ_{max} = 502 and 551 nm for **3-Ru**) consistent with MLCT bands. Notably, the energies associated with the wavelengths of the lowest-energy absorption bands for **1-Ru** (2.94 eV), **2-Ru** (2.26 eV), and **3-Ru** (2.25 eV) reveal a monotonic relationship of decreasing energy (increasing wavelength) for these compounds. This trend can be ascribed to the increasing degree of conjugation as the ligand changes from **bdc** to **tdc** to ^{Ph}**tdc** since the lowest unoccupied molecular orbital (LUMO) of the dicarboxylate ligand is implied by the data to serve as the electron acceptor upon absorption of light by the ruthenium complexes.

Generation and Spectroscopic Characterization of U(V). With the electronic characteristics of **1-UO$_2$** in hand, we next investigated the accessibility of U(V) within this ligand framework. The firm understanding of the absorption characteristics of **1-UO$_2$** afforded by the electronic absorption studies enabled us to begin to bracket the redox potential of **1-UO$_2$** via spectrochemical titrations. Significant reactivity was observed when aliquots of decamethylcobaltocene (Cp^*_2Co; $E_{1/2}$ = −1.91 V vs $Fc^{+/0}$ in MeCN)[44] were added to **1-UO$_2$** in

https://doi.org/10.1021/acs.inorgchem.3c02397
Inorg. Chem. 2023, 62, 16131−16148

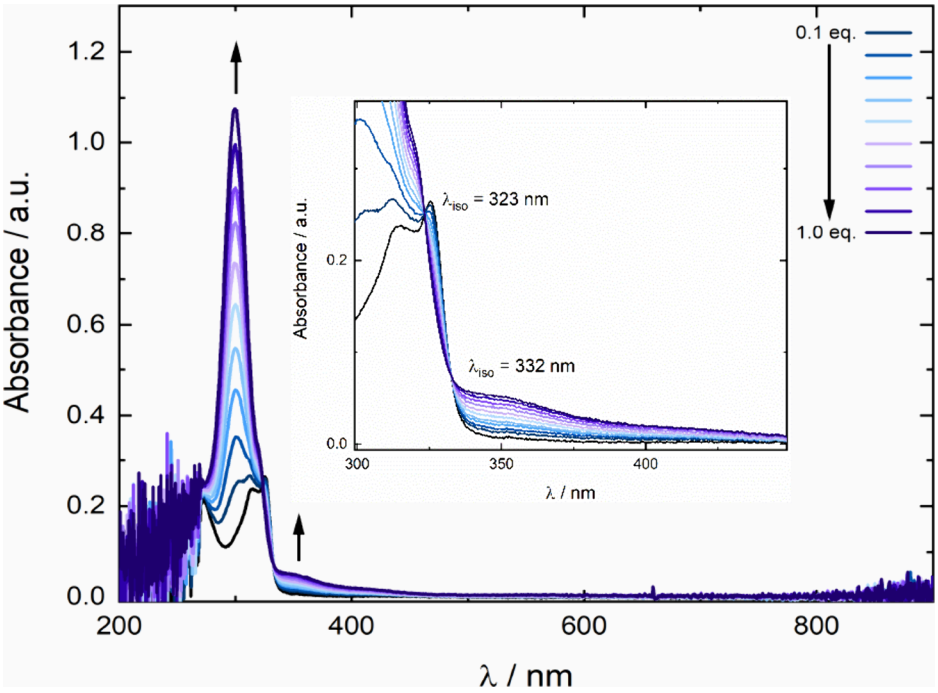

Figure 3. Titration of **1-UO$_2$** in DMF (0.022 mM) with increasing amounts of Cp*$_2$Co showing clean, one-electron reactivity as monitored by electronic absorption spectroscopy.

DMF. A sharp feature around 300 nm, indicative of $[Cp^*_2Co]^+$ generation, can be seen growing in over the course of Cp*$_2$Co additions up to 1 equiv with isosbestic points at 323 and 332 nm, revealing that the desired electron transfer does take place (Figure 3). The reduced species appears to be stable under these conditions; across the time scale of our titration experiments (30 min to ca. 2 h), neither further spectral evolution nor precipitation of solids was observed. We could be confident in the assignment of this process as a 1-electron reduction as only dilution effects were observed when excess Cp*$_2$Co was added, rather than further spectral evolution corresponding to the generation of further equivalents of $[Cp^*_2Co]^+$, (see the SI, Figures S45 and S46).

Conversely, no reactivity of the starting materials was observed when cobaltocene (Cp_2Co; $E_{1/2}$ = −1.33 V vs $Fc^{+/0}$ in CH_2Cl_2)[44] was added to **1-UO$_2$**. No spectral changes were observed aside from dilution effects when aliquots of up to 1 equiv of Cp_2Co were added to **1-UO$_2$** in DMF (see the SI, Figure S49). The lack of reactivity between these two reagents was verified by the observation of a linear relationship between the equivalents of Cp_2Co added and the ratio of absorbance at 325 nm with the concentration of **1-UO$_2$** adjusted for changes in volume (Figures S53). This relationship represents the linearized form of two summed Beer's law relationships for the two separate species that absorb at 325 nm (i.e., Cp_2Co and **1-UO$_2$**); the slope of this line corresponds to the molar absorptivity of Cp_2Co at 325 nm, while the intercept of the line corresponds to the molar absorptivity of **1-UO$_2$** at 325 nm (see the SI, p. S31 for a full discussion of the analysis). The close agreement of the independently determined molar absorptivity values of both species with the slope (slope = 6857 ± 49 M^{-1} cm^{-1} vs ε_{Co} = 7508 ± 63 M^{-1} cm^{-1}; see SI, Figures S53 and S55) and intercept (intercept = 10258 ± 65 M^{-1} cm^{-1}vs ε_U = 10541 ± 168 M^{-1} cm^{-1}; see SI, Figures S53 and S40) of the fitted data support the conclusion that **1-UO$_2$** does not undergo reduction by Cp_2Co in DMF. In an extended effort to detect reactivity, excess Cp_2Co was also added and allowed to stir for nearly ten minutes, but no spectral changes were observed in that experiment either (see the SI, Figures S51 and S52).

In agreement with the evidence for electron transfer to U(VI) obtained in the electronic absorption spectra, the ^{1}H NMR spectrum of a sample of **1-UO$_2$** mixed with a stoichiometric amount of Cp*$_2$Co in d_6-DMSO shows the complete disappearance of the diamagnetic features associated with **1-UO$_2$**. A new feature indicative of the formation of $[Cp^*_2Co]^+$, the oxidized form of Cp*$_2$Co, was observed at 1.68 ppm in addition to other new features that can be assigned to reduced uranium species (see the SI, Figures S5 and S7). Isolated **1-UO$_2$** is diamagnetic, featuring a conventional ^{1}H NMR spectrum containing only three aromatic resonances for the **bdc** ligand and one aliphatic resonance for the equivalent methyl groups of the bound DMSO ligand; this is in accordance with the C_{2v} symmetric nature of the complex in solution (vide supra). Reduction of **1-UO$_2$** with Cp*$_2$Co, however, results in what appears to be eight individual sets of resonances (singlets or multiplets) across a chemical shift range that spans from 5 to 10 ppm (see the SI, Figure S5); the observation of these resonances could be consistent with the generation of multiple species upon reduction at the concentration (12.7 mM) used for the NMR studies. The resonances could be anticipated to be paramagnetically shifted by the in-situ-generated U(V) to which the **bdc** ligand appears to be bound on the basis of both electrochemical and infrared data (vide infra). The reduced species observed by ^{1}H NMR appear(s) stable in solution for at least 24 h as evidenced by the persistence of the spectral features at that time point (see the SI, Figure S6), although we do note that a small amount of gray precipitate was observed in the NMR tube after allowing it to rest in the laboratory overnight. Taken together, we anticipate that these findings indicate that the use of a higher concentration of **1-UO$_2$** in the NMR work (12.7 mM

https://doi.org/10.1021/acs.inorgchem.3c02397
Inorg. Chem. 2023, 62, 16131−16148

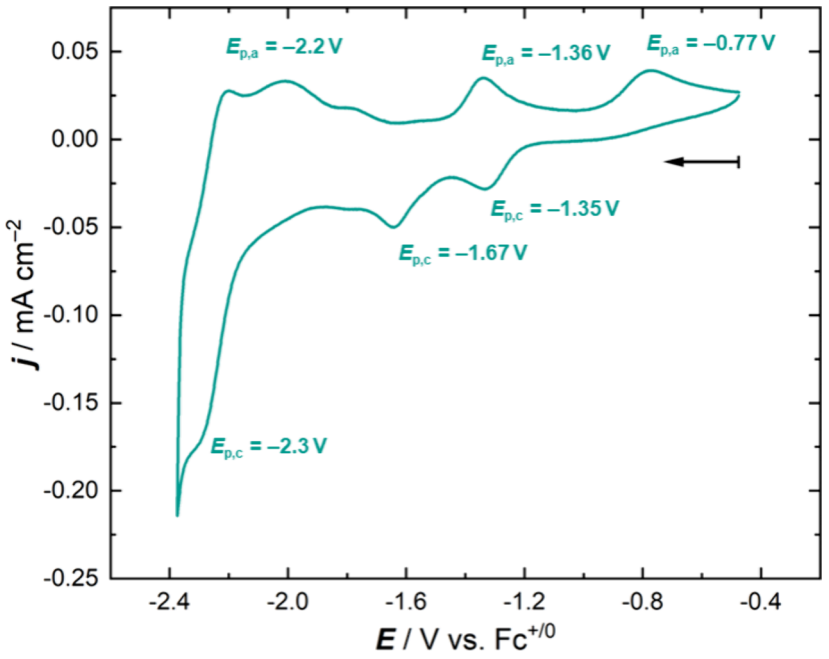

Figure 4. Cyclic voltammetry data for **1-UO$_2$**. Conditions: 0.1 M $[Bu_4N]^+[PF_6]^-$ in DMF; scan rate: 100 mV/s; [**1-UO$_2$**] = 1 mM.

compared to 0.022 mM used in the electronic absorption studies; greater in the NMR case by 577x) could result in additional chemical reactivity; no precipitation behavior was observed in the titration studies with electronic absorption spectroscopy.

Reductive Electrochemistry of 1-UO$_2$. Having bracketed the reduction potential of **1-UO$_2$** with the chemical redox reagents, we also probed the electrochemical response of **1-UO$_2$**. Cyclic voltammetry data for **1-UO$_2$** shown in Figure 4 reveal accessible reduction events at −1.35 and −1.67 V (all potentials quoted vs $Fc^{+/0}$) with corresponding, paired reoxidation events at −0.77 and −1.36 V, respectively. This is in good agreement with the titrations monitored by electronic absorption spectroscopy (vide supra), as both of these reductive features are located at potentials less negative than that of the reduction potential of Cp^*_2Co, but at a more negative value than that of Cp_2Co. Chemical reactivity appears to follow the electrochemical reductions measured in the voltammograms based on the observation of anodically shifted reoxidation waves (ΔE_p values of 580 and 310 mV, respectively) and scan rate-dependent data, which do show only minimal increases in apparent chemical reversibility at faster scan rates (see the SI, Figures S69 and S70). The follow-up reactivity may be a result of the electrochemical conditions, as at least one reduced form of **1-UO$_2$** appears to be persistent in solution on the basis of the stable response observed in the spectrochemical titrations and observation of NMR spectra corresponding to in-situ-generated reduced species (vide supra); however, as precipitate was observed in the NMR study, multiple products appear accessible over longer times and at higher concentrations in chemical work. As expected, cyclic voltammetry data for **1-UO$_2$′** also collected in the DMF electrolyte show an overall quite similar electrochemical profile to **1-UO$_2$** (see the SI, Figure S71), consistent with the similar structures of the two compounds that differ only by the identity of the fifth equatorial ligand prior to dissolution in the DMF-based electrolyte.

Scanning further negative toward the cathodic limit of the conditions in these experiments near −2.4 V revealed another reduction event with $E_{p,c}$ = −2.3 V and corresponding reoxidation with $E_{p,a}$ = −2.2 V; we hypothesize that these features are attributable to a direct ligand-centered reduction process. The smaller value of ΔE_p for this event (100 mV) suggests a chemically reversible process, while the midpoint potential of −2.25 V is relatively similar to the potential measured for the reduction of both **1-Ru** and free **bdc** (both centered at −1.9 V, vide infra). This implies that the generation of a uranium(V) form of **1-UO$_2$** could result in a negative shift of the ligand-centered reduction by 350 mV. This hypothesis is consistent with the formation of the uranium(V) form of **1-UO$_2$**, which would be an anionic species if no chemical reactivity were to occur following electron transfer. Additionally, we note here that the electrochemical data for **1-UO$_2$** and **1-UO$_2$′** indicate that no significant quantity of free **bdc** was generated upon electrochemical reduction of the uranium complexes, as confirmed by the lack of an observable redox signal centered at −1.9 V, suggesting that these species can serve as effective ligands for both the isolated U(VI) and reduced forms of the complexes. This finding is also in accordance with the lack of observation of diamagnetic peaks in the ^{1}H NMR studies attributable to free **bdc** or its presumably accessible deprotonated forms.

To further interrogate the nature of the reduced form(s) of **1-UO$_2$** and the apparent chemical reactivity that follows reduction under electrochemical conditions, increasing amounts of Cp^*_2Co were added to a solution of **1-UO$_2$** in the DMF electrolyte, and cyclic voltammograms were collected on the resulting solution. Upon addition of Cp^*_2Co to the solution, decreased current densities were observed for both the two reduction features and the two oxidation features associated with uranium-centered redox with **1-UO$_2$**; this could be consistent with an overall decrease in the concentration of **1-UO$_2$** (and/or reduction products derived from it) present in solution (see the SI, Figures S72 and S73). Evolution of the cyclic voltammetric data continued across

https://doi.org/10.1021/acs.inorgchem.3c02397
Inorg. Chem. 2023, 62, 16131−16148

additions of up to 1 equiv of Cp^*_2Co (on the basis of the initial concentration of **1-UO$_2$** present in the electrochemical cell); the measured changes in response include the nearly complete disappearance of the reductive feature at −1.35 V and its corresponding oxidation at −0.77 V. The more negative cathodic feature at −1.67 V and corresponding reoxidation wave at −1.36 V persist to some degree, however, suggesting that one reduced/reoxidized form of **1-UO$_2$** can remain in solution. Appealingly, a highly reversible couple corresponding to the $Co^{III/II}$ redox cycling of $Cp^*_2Co^+/Cp^*_2Co$ grows in at −1.91 V; this is consistent with the noted changes being driven in this work by the addition of Cp^*_2Co and electron transfer to **1-UO$_2$**. When more than 1 equiv of Cp^*_2Co was present, the reductive feature at −1.67 V and its related reoxidation wave remained measurable; slight decreases in its current were observed beyond addition of 1 equiv of Cp^*_2Co, a behavior consistent with dilution. The current associated with the $Co^{III/II}$ couple increased after all additions, consistent with buildup of both $Cp^*_2Co^+$ and Cp^*_2Co in solution.

Mirroring the NMR studies, a precipitate formed in the electrochemical cell during the titration; the precipitate became visible beginning around the addition of 0.5 equiv of reductant. At this stage, we anticipate that electron transfer to **1-UO$_2$** in both DMSO (as in the NMR studies) or DMF-based electrolyte (as in the electrochemical work) results in the generation of insoluble species that drive the observable precipitation behaviors. However, loss of the **bdc** ligand from the uranium center does not appear to occur on the basis of both the ^{1}H NMR and electrochemical studies. We anticipate that the observation of precipitates in both the chemical work with NMR and the electrochemical studies could be associated with the relatively higher concentration of uranium present in both cases ($[U]_0$ = 12.7 mM in NMR, 2 mM in electrochemical work) in comparison with UV−visible spectroscopic studies (0.022 mM). Alternatively, the origin of the precipitation behavior could be distinct in both cases. In the case of the latter origin of the precipitation behavior, electrochemical conditions could modulate the speciation of **1-UO$_2$** upon reduction, perhaps through the interaction(s) of nascent reduced species with electrolyte ions. However, considering that all the evidence obtained so far suggests that some reduced species derived from **1-UO$_2$** remain in solution over the time scale of minutes to hours, we pursued further characterization data with infrared and near-infrared spectroscopies to obtain evidence of the oxidation state of species that can persist in solution.

Infrared and Near-Infrared Spectra of U(V). Clean one-electron transfer to **1-UO$_2$** was observed via electronic absorption spectroscopy. Related ^{1}H NMR studies show that at least one form of a reduced complex derived from **1-UO$_2$** persists in DMSO solution after generation (at higher concentration), and related findings were obtained from the electrochemical studies in a DMF-based electrolyte. Importantly, the electrochemical work also indicates that **1-UO$_2$** undergoes electrode-driven reduction at potential(s) positive of those required for ligand-centered reduction. In light of this, we further investigated the site of reduction through the characterization of the in-situ-generated species derived from **1-UO$_2$** in the near-infrared (NIR) region. While 2,2′-bipyridyl and compounds built on this core often display broad, long-wavelength absorption features in this region, it has been well documented that compounds containing U(V) display sharp peaks in the NIR with $\varepsilon \approx 100$ M^{-1} cm^{-1} between 1300 and 1600 nm.[10,32,45] Therefore, we anticipated that distinguishing between a ligand-centered and U-centered reduction could be achieved through the interrogation of NIR spectra of the reduced uranium species. Upon adding 1 equiv of Cp^*_2Co to **1-UO$_2$** in DMF, two sharp features at λ_{max} = 1338 and 1439 nm (7474 and 6949 cm^{-1}, respectively) were observed with molar absorptivity values of ε = 13 and 10 M^{-1} cm^{-1}, respectively (Figure 5). These values agree with the Laporte-

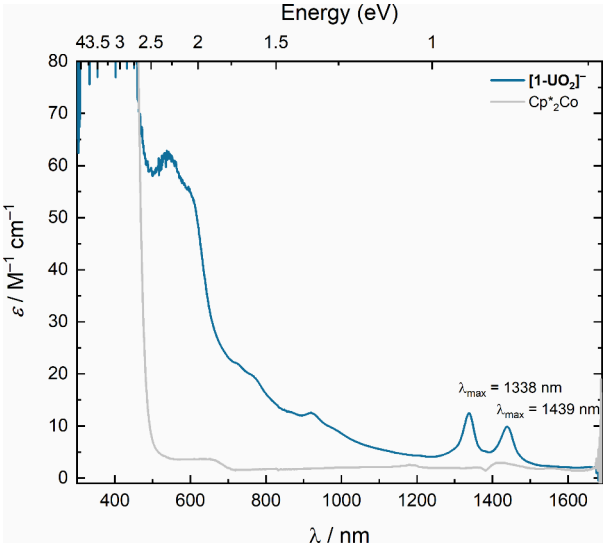

Figure 5. Comparison of NIR spectra of **1-UO$_2$** with 1 equiv of Cp^*_2Co (blue) and Cp^*_2Co (gray) in DMF, supporting the generation of the U(V) oxidation state upon electron transfer.

forbidden nature of these transitions and are similar to other previously reported U(V) NIR features, supporting the generation of U(V) under these conditions.[45]

With this support for the accessibility and identity of U(V) in the **bdc** framework, we analyzed changes in the vibrational spectra between U in the +6 and +5 oxidation states. The asymmetric stretch of the UO_2^{2+} unit in **1-UO$_2$** in DMF can be clearly observed as a strong feature at 912 cm^{-1} when detected by IR; this stretching frequency is in good agreement with previously reported stretches of U(VI) in the *trans*-dioxo environment of uranyl.[46] Upon the addition of Cp^*_2Co to **1-UO$_2$** in DMF, the strong ν_{asym}(U−O) was lost and a small new feature can be observed at 800 cm^{-1} where an asymmetric stretch of U(V)−O might be expected, giving further evidence for the ability of **bdc** to support U(V) in this system (Figure 6).[10,11] Additionally, a complementary infrared spectrum was collected by the addition of Cp^*_2Co to **1-UO$_2$** in DMSO; the spectrum shows retention of a carboxylate C═O stretch, consistent with the interaction of this moiety on the **bdc** ligand remaining bound to uranium. These data provide further evidence of the ability of **bdc** to support U(V) and remain bound to the studied, presumably the anionic form of the complex (see SI, Figure S29).

Although the structure and detailed composition of the reduced form(s) of **1-UO$_2$** on which the spectroscopic and electrochemical experiments could be carried out are not known at this time, we can conclude from the assembled evidence that the species retain(s) the bound **bdc** ligand and feature(s) uranium in the +V oxidation state. As these features appear established at this time, we have elected to denote the reduced species (or mixture of species) detected in the

https://doi.org/10.1021/acs.inorgchem.3c02397
Inorg. Chem. 2023, 62, 16131−16148

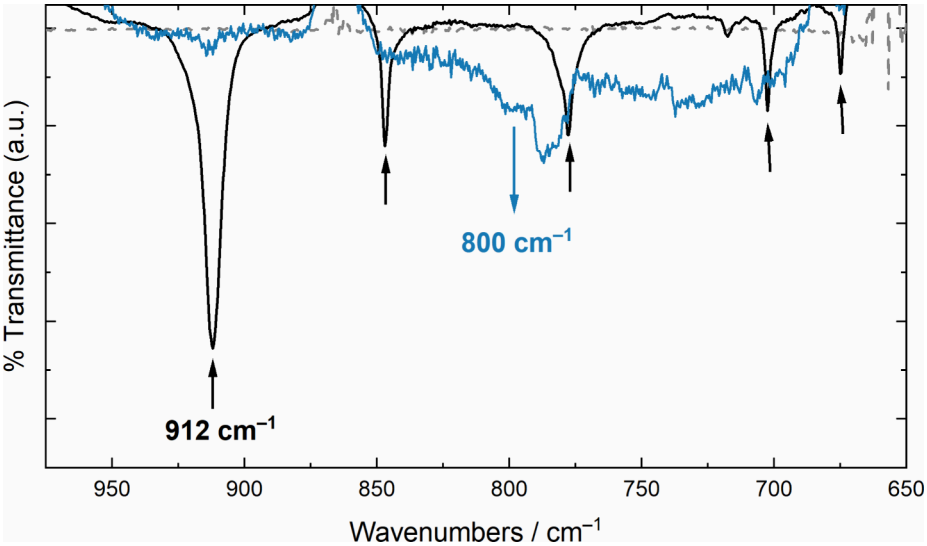

Figure 6. Comparison of solution IR spectra collected for **1-UO$_2$** (black) and a sample obtained by mixing of **1-UO$_2$** with 1 equiv of Cp*$_2$Co (blue) in DMF, supporting the generation of the U(V) oxidation state upon electron transfer to **1-UO$_2$**.

spectroscopic and electrochemical work as [**1-UO$_2$**]$^-$, in accordance with the measurements implying the presence of U(V) and the retention of the bound **bdc** ligand. Regarding the precipitation behaviors measured in select experiments, one reviewer of this study helpfully suggested that the two sequential, presumably uranium-centered reductions measured in the electrochemical work could suggest the accessibility of the U(IV) oxidation state in the DMF-based electrolyte. U(IV) species could be anticipated to be more reactive than their U(VI) or U(V) counterparts, meaning that they could contribute to the formation of precipitates through further reactivity. Thus, we note here that the observation of spectroscopic and electrochemical features corresponding to the generation of U(V) species does not preclude disproportionation behaviors or involvement of U(IV) species in the formation of the precipitates that could be seen visually during select experiments.

Reductive Electrochemistry of Ruthenium Complexes. As mentioned previously, ruthenium complexes of **bdc** and related polypyridyl dicarboxylates **tdc** and ^{Ph}**tdc** were synthesized as control compounds to aid in the assignment of the site of reduction in **1-UO$_2$**. Additionally, the Ru(II) complexes have beneficial properties compared with the free ligands in that they are more soluble and could be less likely to engage in stacking interactions with the working electrode surface; we have found that these difficult properties of **H$_2$bdc**, **H$_2$tdc**, and **H$_2$**^{Ph}**tdc** preclude direct, extensive solution-phase studies. Prior work with Ru(II) complexes of **bdc** and **tdc** has demonstrated that these ligands can support complexes showing rich redox chemistry, but investigations have focused entirely, to the best of our knowledge, on their oxidative electrochemical properties.[17,24,30] In particular, electrochemical data show that such complexes can undergo sequential, metal-centered oxidations that are chemically reversible, giving access to the Ru$^{III/II}$ and Ru$^{IV/III}$ processes and underpinning the ability of these complexes to serve as oxidation catalysts.[18,24,30] On the other hand, the reductive electrochemical properties of Ru(II) complexes of **bdc**, **tdc**, and ^{Ph}**tdc** have not been reported. Elucidation of these properties could be useful, particularly because ruthenium is not known to readily undergo reduction beyond the +2 oxidation state;[25] thus, any reduction processes measured might be more readily confirmed as ligand-centered in nature.[47]

In line with our expectations based on prior work with complexes containing the bipyridyl core motif, the cyclic voltammogram (CV) of **1-Ru** reveals that there is a single accessible reduction event in dimethylformamide-based electrolyte with a midpoint reduction potential ($E_{1/2}$) of −1.90 V vs Fc$^{+/0}$ (Figure 7; Figure S73 in the SI). This process appears to be chemically quasi-reversible, based on the

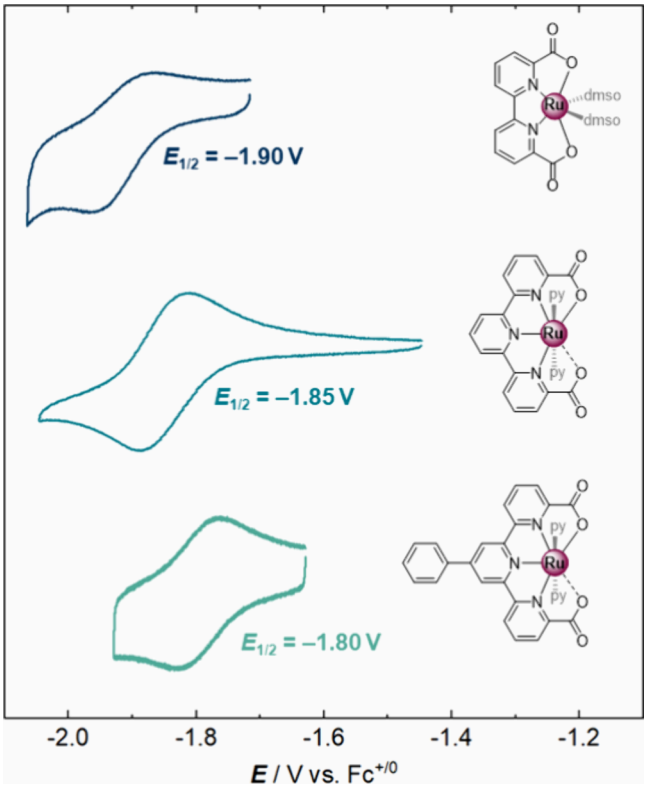

Figure 7. Cyclic voltammetry spectra of **1-Ru** (top), **2-Ru** (middle), and **3-Ru** (lower). Conditions: 0.1 M [Bu$_4$N]$^+$[PF$_6$]$^-$ in DMF; scan rate: 100 mV/s; [Ru] = 1 mM in all cases.

https://doi.org/10.1021/acs.inorgchem.3c02397
Inorg. Chem. 2023, 62, 16131−16148

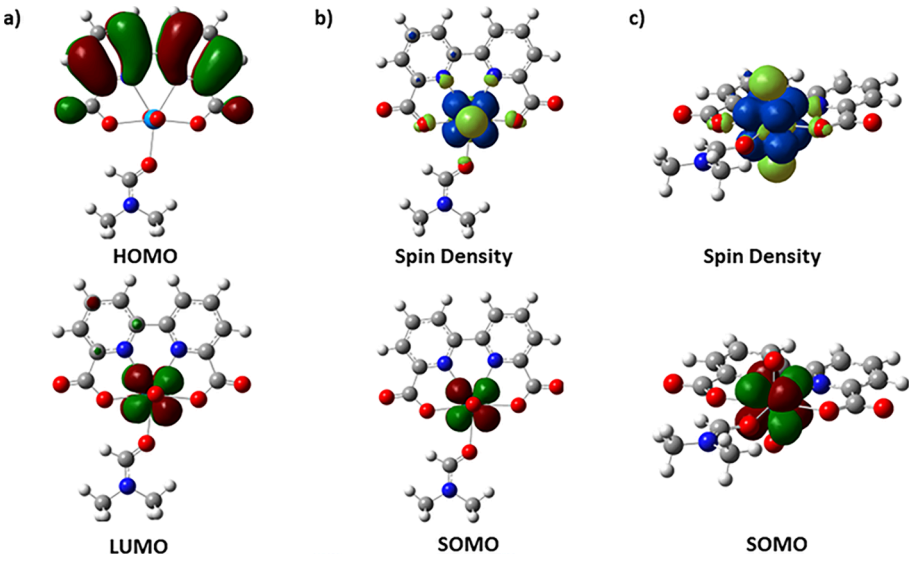

Figure 8. (a) HOMO and LUMO of **1-UO$_2$′**; (b) Spin density and SOMO of [**1-UO$_2$′**]$^-$; (c) alternative views of spin density and SOMO of [**1-UO$_2$′**]$^-$.

attenuated peak current associated with reoxidation of the reduced form of the complex (Figure 7). Scan rate-dependent data confirm, however, that both the oxidized and reduced forms of **1-Ru** are freely diffusing in solution, consistent with the solubility of **1-Ru** in DMF (see the SI, Figure S81). CVs collected of **2-Ru** and **3-Ru** in the DMF electrolyte reveal similar reduction processes with $E_{1/2}$ values of −1.85 and −1.80 V vs $Fc^{+/0}$, respectively (see Figure 7). However, these processes appear significantly more chemically reversible in nature, as the cathodic and anodic peak currents are similar for each of these complexes at a variety of scan rates. As in the case of **1-Ru**, scan rate-dependent data for **2-Ru** and **3-Ru** confirm the diffusional nature of the oxidized and reduced forms of these compounds in the DMF electrolyte (see the SI, Figures S82−S85).

Notably, there is a uniform positive shift of the estimated $E_{1/2}$ values for **1-Ru**, **2-Ru**, and **3-Ru** (−1.90, −1.85, and −1.80 V, respectively). This shift in the reduction potentials to more positive values is consistent with ligand-centered reduction of the complexes, considering that (i) the expanded π-systems of **tdc** and ^{Ph}**tdc** should enable reduction of these species at more positive potentials than that of smaller **bdc** and that (ii) ^{Ph}**tdc** contains a terpyridyl core with an additional conjugated phenyl ring that should enable easier reduction of this ligand in comparison to **tdc**. Indeed, the cyclic voltammetry data shown in Figure 7 confirm this model of the reduction potentials of the complexes and suggest that the processes measured in all cases are ligand-centered.

In line with these results for the ruthenium complexes of **bdc**, **tdc**, and ^{Ph}**tdc**, preliminary CV data collected with the free diprotic ligands display single reduction processes in all cases. However, unlike the metal complexes, the free ligands undergo chemically quasi-reversible reductions with $E_{1/2}$ values that are similar in each case and centered near −1.9 V (see the SI, Figures S74−S79). In light of the measurement of similar reduction potentials for each of the free ligands, we hypothesize that the extent of the effective conjugation of each species in solution may be quite different from those measured in the corresponding ruthenium complexes (vide supra), leading to similar reduction potentials. This may be attributable to greater nonplanarity of the free ligands, diminishing the effectiveness of conjugation that can be confirmed in the metal complexes. Additionally, based on the poorer apparent chemical reversibility of the reduction waves measured for the free organic molecules, chelation of the ligands to ruthenium results in increased stability of the reduced forms of the ligands, particularly in the case of **tdc** and ^{Ph}**tdc**. However, as each free ligand and metal complex can undergo single reduction processes, the available data do suggest that the reduction events are predominantly centered on the conjugated organic ligand core in all cases.

Computational Studies of Reduced Complexes. DFT calculations were used to probe the electronic structure of the complexes prepared in this study and their reduced analogues to aid in the differentiation between metal- and ligand-centered reduction. Beginning with coordinates of each complex derived from structural data from X-ray diffraction analysis, optimized geometries for neutral and reduced forms of the complexes were computed (see SI, pp. S53 and S65 for the Cartesian coordinates). Based on these structures, highest occupied molecular orbitals (HOMOs), lowest unoccupied molecular orbitals (LUMOs), singly occupied molecular orbitals (SOMOs), and spin density plots were visualized to gain insight into the distribution of electron density in the reduced species (e.g., Figure 8). Spin density is defined as the difference between ρ_α and ρ_β (i.e., the density of α-spin electrons minus the density of β-spin electrons). Therefore, blue regions correspond to an excess of α density and the light-green regions to an excess of β density (e.g., top right structure in Figure 8). Furthermore, we remind the reader that an orbital is not a density (the latter in DFT is obtained as the sum of the modulus squared of the occupied orbitals), and the colors in the orbital isodensity surfaces only reflect the sign of the orbital in a certain region of space; however, the sign value is arbitrary as it disappears when the density is computed. Nonetheless, one would expect that the shape of the spin density and that of the SOMO in the reduced species to be similar if the extra electron is mainly localized in the SOMO.

Calculations on **1-UO$_2$′** reveal a distinctly metal-based SOMO upon reduction of the parent complex by 1e$^-$.

https://doi.org/10.1021/acs.inorgchem.3c02397
Inorg. Chem. 2023, 62, 16131−16148

Employing the coordinates from the crystal structure of **1-UO$_2$′**, HOMO and LUMO are visualized for the neutral form of the complex, as shown in Figure 8. While the HOMO is primarily on the ligand, the LUMO is metal-centered and becomes populated upon the addition of one electron. This is consistent with the high-valent nature of U(VI) and the propensity for this system to undergo reduction, as discussed above. In the reduced form of **1-UO$_2$′**, the orbital containing the unpaired electron and the spin density bears a strong resemblance to the $f_{z(x^2-y^2)}$ orbital from the general 5*f* set.[48] The spin density is localized on the uranyl ion with significant β electron density extending out onto the oxo groups of the uranyl moiety, an observation consistent with the multiple-bond character of the uranyl ion and the recognized propensity of uranium(V) species to display greater oxo-centered basicity than their uranium(VI) counterparts.[10] Charge analysis finds that 48% of the charge in [**1-UO$_2$′**]$^-$ is accounted for by the uranium center itself, whereas only 30% can be accounted for by atoms contained in the **bdc** framework (see the SI, Table S11).

In addition to these observations relating to the calculated orbitals, significant structural changes were computationally observed upon reduction that support a uranium-centered reduction process. All of the U−N and U−O interactions that tether uranyl to **bdc** lengthen upon reduction (with an average increase of 0.064 Å for the U−N bonds and 0.122 Å for the U−O bonds), indicating that the uranyl unit becomes more electron-rich. On the other hand, computing the Ψ_M parameter for the U metal centers in **1-UO$_2$′** and [**1-UO$_2$′**]$^-$ reveals that the value of this parameter does not change significantly upon reduction (from 0.007 for **1-UO$_2$′** to 0.001 for [**1-UO$_2$′**]$^-$), indicating that the U center remains situated in the planar tetradentate pocket provided by **bdc** even upon generation of the monocationic UO_2^+. Upon reduction, the monocationic nature of UO_2^+ is further evident in the calculated elongation of the U−O_{oxo} distances by 0.058 Å for both oxo oxygens, a value consistent with elongations measured in prior structural work.[10] Additionally, consistent with the metal-centered nature of the reduction of **1-UO$_2$′** but in contrast to the ligand-centered reduction behavior of **1-Ru** (vide infra), the bipyridyl C5−C6 distance in [**1-UO$_2$′**]$^-$ is only slightly contracted compared to the neutral **1-UO$_2$′** (Δd_{C5-C6} = 0.006 Å; see the SI, Table S12), highlighting the capability of **bdc** to support uranium species in lower valencies. Indeed, the electrochemical data suggest that the ligand-centered reduction of species derived from **1-UO$_2$** or **1-UO$_2$′** occurs at potentials significantly more negative than those required for the reduction of U(VI) to U(V).

Time-dependent density functional theory calculations (TD-DFT) based on the M06L functional were carried out on the reduced species [**1-UO$_2$′**]$^-$ to confirm the presence of transitions originating from orbitals derived from *f* parentage. Indeed, the 20 lowest transitions of the same spin symmetry as the ground state involve *f* orbitals (Table S13). Some of these transitions have small but nonzero oscillator strength in the near-IR region, which is in accordance with the measured spectral properties of [**1-UO$_2$**]$^-$ from the spectrochemical titrations. Although these calculations are somewhat limited in scope, as they ignore relativistic effects such as spin−orbit coupling that could reveal other transitions with non-negligible intensity, they support the interpretation of the experimental data in that both charge transfer transitions and transitions in the near-IR were measured, which could correspond to *f*-to-*f* transitions. Similar results were also obtained at the TD-B3LYP and TD-CAM-B3LYP levels of theory (see Tables S14, S15 and Figure S93).

In the case of the neutral form of **1-Ru**, the HOMO resides primarily on the metal, with a small amount of electron density extending to the atoms that are directly coordinated to Ru(II). The LUMO, on the other hand, is ligand-centered and becomes populated with electron density upon reduction, as seen in the SOMO and spin density maps (Figure 9).

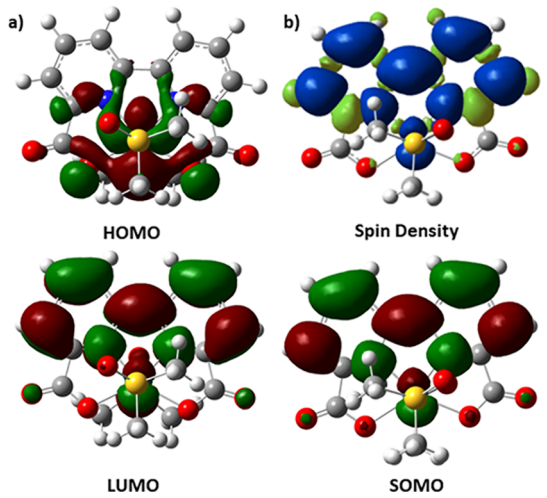

Figure 9. (a) HOMO and LUMO of **1-Ru**; (b) Spin density and SOMO of [**1-Ru**]$^-$.

Consistent with ligand-centered reduction and the conjugated nature of the bipyridyl core of **bdc**, structural changes in the ligand were also calculated, including most notably contraction of the C5−C6 distance (contraction of 0.043 Å from **1-Ru** to [**1-Ru**]$^-$; see the SI, Table S12).[49] Additionally, atomic charge analysis shows large increases in the charge density of the pyridyl rings compared to ruthenium and the axial DMSO ligands, where the charge on the pyridyl rings accounts for 74% of the single additional anionic charge in [**1-Ru**]$^-$ (see the SI, Table S11). TD-DFT calculations also confirmed a tail at longer wavelengths for [**1-Ru**]$^-$ compared to its neutral analogue, in line with the spectral properties anticipated for a bipyridine anion with radical-like character in the reduced compound and consistent with experimental spectra (see Figures S94−S99, where calculations are performed with all density functionals).

The DFT calculations of **2-Ru** and **3-Ru** yielded similar evidence of the preference for ligand-centered reduction (see the SI, Figure S92 for visualizations of **2-Ru** and [**2-Ru**]$^-$). In both cases, the HOMO remains primarily on Ru(II) and the atoms directly bonded to it with the bulk of the LUMO residing on the ligand (Figure 10). Upon reduction, the SOMO again appears to be populated by a ligand-centered radical, but notably, a nonsymmetric distribution of electron density is observed for the **tdc** and ^{Ph}**tdc** complexes. In particular, the ligand-centered electron spin density is greater on the region of the complex that bears the carboxylate functionality positioned in greater conjugation with the terpyridyl π-system and coordinated to ruthenium. This carboxylate group is associated with a short Ru−O distance of ca. 2.2 Å in the data from XRD (see the SI, Table S16). Thus, the in-plane conjugation of the Ru-bound carboxylate

https://doi.org/10.1021/acs.inorgchem.3c02397
Inorg. Chem. 2023, 62, 16131−16148

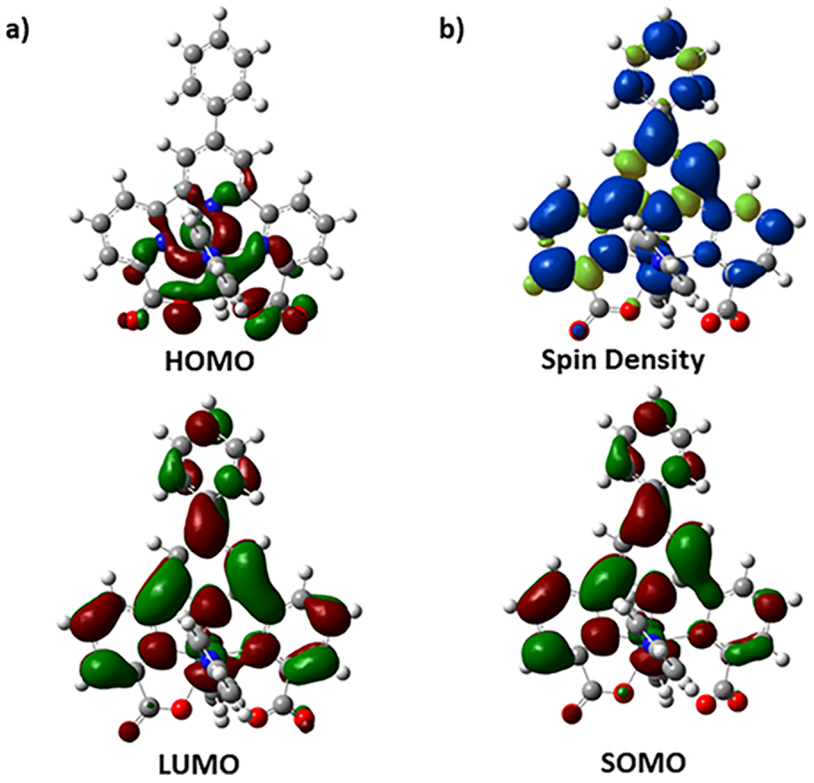

Figure 10. (a) HOMO and LUMO of **3-Ru**; (b) spin density and the SOMO of $[\mathbf{3\text{-}Ru}]^-$.

group affords an electron-withdrawing effect with a portion of unpaired spin density present in the carboxylate group that is in conjugation with the terpyridyl core. On the other hand, less electron spin density was found on the pyridyl ring adjacent to the unbound carboxylate that is formally not metal-bound (Ru···O distance of ca. 3.7 Å; see Table S16). This arrangement allows the formally anionic carboxylate to repel the nascent electron spin density placed into the LUMOs of **2-Ru** or **3-Ru**, resulting in the nonsymmetrical delocalization of electron spin density in these systems. Therefore, the relative orientation of the carboxylate groups with respect to the ligand plane has the net effect of localizing most of the charge density on the pyridyl rings containing N1 and N2 (and away from the N3 ring) in the reduced forms of both **2-Ru** and **3-Ru**. In the case of $[\mathbf{2\text{-}Ru}]^-$, the charge density resides at 34% on the pyridyl containing N1, 33% on the pyridyl containing N2, and only 9% on the pyridyl containing N3. For $[\mathbf{3\text{-}Ru}]^-$, the charge density resides 26, 40, and 11% on the rings containing N1, N2, and N3, respectively (see the SI, Table S11); the additional phenyl group of ^{Ph}**tdc** stabilizes the spin density on the N2 ring through its conjugated structure.

Further support for the localization of most of the unpaired spin on a bipyridyl core within **tdc** or ^{Ph}**tdc** is provided by the determination of a nonsymmetric contraction of the inter-ring linking C−C bonds (Δd_{C5-C6} = 0.037 Å; $\Delta d_{C10-C11}$ = 0.004 Å) (see the SI, Table S12). In the case of $[\mathbf{2\text{-}Ru}]^-$, the C5−C6 distance is contracted by 0.037 Å compared to **2-Ru**, which compares well with an experimental value that we have measured (Δd_{C5-C6} = 0.048 Å) for a set of related [Cp*Rh(bpy)] (Cp* = pentamethylcyclopentadienyl) complexes displaying significant reduced ligand character.[50] Similar to $[\mathbf{2\text{-}Ru}]^-$, a contraction of 0.028 Å was observed in the C5−C6 bond of $[\mathbf{3\text{-}Ru}]^-$. Taken together, these findings support the hypothesis that the first reductions measured for **1-Ru**, **2-Ru**, and **3-Ru** are ligand-centered in nature. Also, for these two complexes and for **1-Ru**, TD-DFT spectra reveal a tailing absorption at longer wavelengths in the simulated spectra computed for the reduced species, by comparison to the spectra for the neutral species, in all choices of density functionals (see the SI, Figures S94−S99).

DISCUSSION

Prior structural and metal-binding equilibrium studies in aqueous media have suggested that complexes of U(VI) and **bdc** could be formed, but no synthetic route or characterization data for these complexes under nonaqueous conditions have been reported. With the properties of these species partially established in the prior work, we were encouraged to target the development of a protonolysis-driven synthetic strategy for **bdc** complexes of uranyl. Under nonaqueous conditions, we were able to isolate the molecular complex **1-UO_2** and probe the ability of **bdc** to support uranium in the +5 oxidation state. Indeed, the addition of 1 equiv of Cp^*_2Co, a well-known one-electron reductant, resulted in the clean formation of a reduced species whose spectral features are indicative of the formation of U(V). The spectra given here support the oxidation state assignment of U as +5 and add to the limited reports of U(V) complexes, which can still be considered to be a frontier area in the *f*-element community.[11,14] We also extended the characterization of the **bdc**-ligated species in this report to their electrochemical behavior. In particular, we note that preliminary evidence from this work suggests that the U(V) forms of these compounds are significantly more promiscuous in their reactivity and prone to speciation than the stable U(VI) starting materials on the basis of the features in voltammetry, implying that chemical reactivity occurs upon reduction. However, the observation that these complexes undergo uranium-centered reductions at

https://doi.org/10.1021/acs.inorgchem.3c02397
Inorg. Chem. 2023, 62, 16131−16148

potentials well positive of the practical limit for work in DMF-based electrolyte and that U(V) is accessible in this ligand framework suggest that **bdc** could be a useful ligand platform for further studies of reduction-induced reactions of higher-valent uranium or other actinyls.

In our study of the reductive chemistry of uranyl complexes supported by the polypyridyl dicarboxylate ligands, we anticipated that a valuable comparison could be made between the U complexes and their Ru-ligated analogs to aid in the distinction between metal- and ligand-centered reduction, as the reduction would likely be ligand-centered when Ru(II) is the metal center in question. While prior electrochemical studies of polypyridyl dicarboxylate complexes of ruthenium have established the ability of these ligands to support metals under highly oxidizing conditions, even allowing for the multiple metal-centered oxidations involved in catalysis of water oxidation, the reductive electrochemical properties of these ligands were not reported until now. We investigated the electronic properties of **1-Ru**, **2-Ru**, and **3-Ru** and found that the profiles of these species indicate the presence of an accessible ligand-based LUMO that shifted to lower energies as the extent of conjugation increases in the ligand backbone. While differences in coordination environments between **1-Ru**, **2-Ru**, and **3-Ru** are evident both spectroscopically and structurally, insight from computational results indicates a comparison of these complexes is useful; electron density associated with transfer of $1e^-$ to these complexes was confirmed to undergo delocalization across each conjugated system, with greater conjugation driving more extensive delocalization in the **2-Ru** and **3-Ru** systems in particular. However, a bipyridyl-like motif was predicted by the calculations to be preserved at the core of each reduced complex; reduction of the ligand in each case was shown to result in lengthening of one inter-ring bond (C5−C6) but not the adjacent inter-ring distance. This observation made comparison of all three complexes in the computational studies especially gratifying in this case, as these results agree well with experimental electrochemistry. More generally, the observation of accessible redox couples for the Ru(II) complexes in electrochemical investigations and the apparent uniform positive shift of these $E_{1/2}$ values as the conjugation of the ligand backbone is extended are indicative of ligand-based reduction in the Ru(II) complexes, especially since ruthenium is not known to readily undergo reduction beyond the +2 oxidation state.[25,26] Appealingly, the computational work provides a direct link between our work with the polypyridyl dicarboxylate complexes and prior experimental work with systems featuring reduced ligand character in that the quantitative structural metrics from experimental investigation of the noted bipyridyl systems compare quite well with the computationally derived metrical data presented in the current work.

Finally, while the **bdc** ligated species of uranyl were soluble and could be characterized by solution-phase techniques, the more extensive conjugation of **H_2tdc** and **$H_2{}^{Ph}$tdc** appears to drive the formation of highly insoluble material upon reaction with uranyl precursors in both cases. This result is likely also attributable to the anticipated pentadentate nature of the **tdc** and **^{Ph}tdc** frameworks in that protonolysis reactivity would generate neutral complexes of $[UO_2]^{2+}$ supported by the dianionic ligands that could be quite insoluble in polar organic solvents. We note that prior work from Mazzanti and co-workers has proven the utility of **tdc**-like frameworks for studies of lanthanide chemistry;[51] thus, the current work suggests that additional derivatization of the **tdc** core with solubilizing alkyl groups could engender greater solubility for solution-phase studies. Further exploration of the coordinative properties of dicarboxylate ligands in actinide chemistry is called for, in any case, as both U(VI) and U(V) appear to bind stably to **bdc**, even in coordinating media.

CONCLUSIONS

We have prepared and characterized two U(VI) complexes supported by polypyridyl dicarboxylate ligand **bdc**. Complementary electronic absorption spectra and signature features in the near-infrared spectral region show that the site of the first reduction in such complexes is uranium-centered, giving rise to a U(V) complex supported by **bdc**. This was distinguished from a ligand-centered process by comparison of the reductive chemistry of **1-UO_2** with control Ru(II) compounds, whose first accessible redox process is ligand-centered in these complexes. Reductive electrochemical studies of **1-UO_2**, however, reveal that the uranium(V) complexes are likely less stable in solution than their uranium(VI) counterparts and undergo speciation, possibly involving the formation of secondary species deserving of investigation in future work. Solid-state structural data from X-ray diffraction analysis of both U(VI) and Ru(II) complexes in this family highlight the useful flexibility of **bdc**, which enables it to ligate these metals of differing sizes and oxidation states despite its highly conjugated nature. This work represents the first report of the reductive characteristics of polypyridyl dicarboxylate ligands and their metal complexes, highlighting their unique ability to support reduced forms of uranyl and building on their robust chemistry from the field of redox catalysis. As these sturdy ligands are resistant to reduction until rather negative potentials and display notable carboxylate-influenced spin density properties upon reduction, polypyridyl dicarboxylates represent an exciting family of ligands for future investigations under reducing conditions.

EXPERIMENTAL SECTION

General Considerations. All manipulations were carried out in dry N_2-filled gloveboxes (Vacuum Atmospheres Co., Hawthorne, CA) or under a N_2 atmosphere using standard Schlenk techniques unless otherwise noted. All solvents were of commercial grade and dried over activated alumina using a PPT Glass Contour (Nashua, NH) solvent purification system prior to use and were stored over molecular sieves. 2,2′-Bipyridyl, 2,2′:6′,2″-terpyridyl, 2-acetylpyridine, and benzaldehyde were purchased from Aldrich, Oakwood Chemical, and Sigma-Aldrich, respectively, and were used without further purification. $RuCl_2DMSO_4$,[52] 2,2′-bipyridyl-6,6′-dicarboxylic acid,[20] 2,2′:6′,2″-terpyridyl-6,6″-dicarboxylic acid,[53] 4′-phenyl-2,2′:6′,2″-terpyridyl,[54] 4′-phenyl-2,2′:6′,2″-terpyridyl-N,N-dioxide,[55] 4′-phenyl-2,2′:6′,2″-terpyridyl-6,6″-dicarbonitrile,[55] **1-Ru**,[29] and **2-Ru**[30] were prepared according to literature procedures. Deuterated solvents were purchased from Cambridge Isotope Laboratories.

^{1}H and ^{13}C NMR spectra were collected on 400 or 500 MHz Bruker spectrometers (Bruker, Billerica, MA, USA) and referenced to the residual protio-solvent signal.[21] Infrared spectra were collected on the benchtop in an open atmosphere using a Shimadzu IRSpirit Fourier Transform infrared spectrometer in transmission mode using KBr solid pellets or with a solution cell. Electronic absorption spectra were collected with an Ocean Optics Flame spectrometer equipped with a DH-Mini light source (Ocean Optics, Largo, FL, USA) using quartz cuvettes. Experimental high resolution mass spectrometry data were collected on an LCT Premier mass spectrometer equipped with a quadrupole time-of-flight mass analyzer and an electrospray ion

https://doi.org/10.1021/acs.inorgchem.3c02397
Inorg. Chem. 2023, 62, 16131−16148

source. Predicted mass spectrometry data were obtained from the PerkinElmer Informatics ChemDraw Professional Suite. Elemental analyses were performed by Midwest Microlab, Inc. (Indianapolis, IN, USA), the University of Southern California (Los Angeles, CA, USA), and the CENTC Elemental Analysis Facility at the University of Rochester.

X-ray Crystallography. Crystals were mounted using Paratone oil with MiTeGen loops and placed under a cold nitrogen stream for data collection. For **1-UO$_2$′**, low-temperature (120 K) X-ray data were collected using 0.5° ω- or φ-scans on a Bruker D8 3-circle diffractometer with a PHOTON-II detector. X-rays were provided by a fine-focus Mo-sealed tube running at 50 kV and 35 mA (Mo Kα = 0.71073 Å). All diffractometer manipulations for **1-UO$_2$′**, including data collection, integration, and scaling, were carried out using the Bruker APEX4 Software Suite.[56] For **3-Ru**, low-temperature (145 K) X-ray data were collected using 0.5°-wide ω- or φ-scans on a Bruker D8 Venture diffractometer with a Photon III CPAD detector equipped with Helios high-brilliance multilayer mirror optics. X-rays were provided by an IμS 3.0 Microfocus Mo sealed tube running at 50 kV and 1.4 mA (Mo Kα = 0.71073 Å). All data manipulations for **3-Ru** were carried out using the Bruker APEX4 Software Suite.[57] The data set for **3-Ru** was corrected for absorption using the multiscan method by SADABS, while a numerical face-indexed absorption correction was used for **1-UO$_2$′**.[58] SHELXT was used to solve each structure using intrinsic phasing methods.[59] Final stages of weighted full-matrix least-squares refinement were conducted using F_o^2 data with SHELXL in SHELXle.[60]

All non-hydrogen atoms were refined anisotropically. Nonmethyl hydrogen atoms bonded to carbon in each complex were fixed at idealized riding model sp^2- or sp^3-hybridized positions with C−H bond lengths of 0.95−0.99 Å. Methyl groups were incorporated into the structural models either as sp^3-hybridized riding model groups with idealized "staggered" geometry and a C−H bond length of 0.98 Å or as idealized riding model rigid rotors (with a C−H bond length of 0.98 Å) that were allowed to rotate freely about their N−C bonds in least-squares refinement cycles. The isotropic thermal parameters of the idealized hydrogen atoms in all structures were fixed at values 1.2 (nonmethyl) or 1.5 (methyl) times the equivalent isotropic thermal parameter of the carbon atom to which they are covalently bonded. The relevant crystallographic and structure refinement data for structures **1-UO$_2$′** and **3-Ru** are listed in Table S17.

Computational Details. All calculations were performed with a development version of the Gaussian suite of programs using density functional theory with Grimme's D3 dispersion correction.[61,62] Ruthenium complexes were treated with the revised Minnesota 06 (M06L) functional, which has been shown to give good agreement with experimental results for geometric structure parameters (Ru−C/O).[63] The def2TZVP basis set with Stuttgart/Dresden (SDD) effective core potential (ECP) was used for Ru in all calculations and 6-31++G (d, p) was used for the remaining atoms H, C, N, O, and S.[64,65] Geometry optimization of the uranium complexes was performed using the B3LYP functional and treated with small-core Stuttgart/Dresden ECPs within the quasi-relativistic Wood-Boring correction.[66,67] ECP60MWB was used to match the valence basis set for uranium, and the remaining atoms (H, C, N, and O) were treated with the 6-31g(d) basis set.[65,68,69] The solvent (DMF) was modeled by the solvation method based on density (SMD).[70] All geometry optimizations were carried out in solution. Geometries of the neutral compounds were optimized as singlets, and the reduced compounds were optimized as doublets. Plots of calculated Kohn−Sham orbitals were generated using Gaussview (v. 5.0.8) with an isovalue of 0.04 and spin density maps with an isovalue of 0.002. Note that although the calculations discussed in the main text used the optimal functional for each metal complex based on the available literature, we also performed single-point cross calculations using the other functional for the complexes of the two metals and confirmed the same qualitative picture. TD-DFT calculations were performed at the corresponding level of theory and basis set as for the ground-state calculations.

Electrochemistry. Electrochemical experiments were carried out in a nitrogen-filled glovebox. Tetra(*n*-butylammonium) hexafluorophosphate (Sigma-Aldrich, electrochemical grade; 0.1 M in DMF) served as the supporting electrolyte for all experiments. Measurements were made with a Gamry Reference 600 Plus potentiostat/galvanostat using a standard three-electrode configuration. The working electrode was the basal plane of highly oriented pyrolytic graphite (HOPG) (GraphiteStore.com, Buffalo Grove, IL; surface area: 0.09 cm^2), the counter electrode was a platinum wire (Kurt J. Lesker, Jefferson Hills, PA; 99.99%, 0.5 mm diameter), and a silver wire immersed in the electrolyte served as a pseudoreference electrode (CH Instruments). The reference was separated from the working solution by a Vycor frit (Bioanalytical Systems, Inc.). For all uranium complexes, a platinum wire directly immersed in the working solution was used as a quasi-reference electrode. Ferrocene (Sigma-Aldrich, twice-sublimed; 0.1 M) was added to the electrolyte solution at the conclusion of each experiment, and the midpoint potential of the ferrocenium/ferrocene couple (denoted as $Fc^{+/0}$) served as an external standard for comparison of the recorded potentials.

Synthetic Procedures. *Preparation of UO$_2$bdc Complexes 1-UO$_2$ and 1-UO$_2$′.* **1-UO$_2$** is a known material characterized previously by UV−visible spectroscopy and single-crystal X-ray diffraction by Rao and co-workers.[15] In the current work, we developed methods for the preparation of **bdc**-ligated uranyl complexes and provided relevant characterizations of each complex.

1-UO$_2$. To a stirring solution of 2,2′-bipyridyl-6,6′-dicarboxylic acid (0.049 g, 0.2 mmol) in a minimal amount of DMSO in a 20 mL scintillation vial was added uranyl acetate dihydrate (0.085 g, 0.2 mmol) as a solid in open air, instantly turning the solution a vibrant yellow color. The solution was stirred overnight at room temperature. The next day, the yellow solution was transferred to an Erlenmeyer flask and flooded with diethyl ether (∼400 mL). The flask was covered with Parafilm and cooled to 4 °C for at least 24 h. The precipitate was collected via vacuum filtration and washed with diethyl ether to yield **1-UO$_2$** as a pale-yellow solid (0.118 g, 99%). ^{1}H NMR (500 MHz, d_6-DMSO) δ (ppm): 9.27 (d, 2H, J = 7.9 Hz), 8.76 (t, 2H, J = 7.8 Hz), 8.68 (d, 2H, J = 7.7 Hz), 2.54 (s, 6H, J = 7.3 Hz). ^{13}C{^{1}H} NMR (126 MHz, d_6-DMSO) δ (ppm): 170.95, 157.21, 156.18, 143.61, 127.28, 126.46. IR spectroscopy (KBr) ν(cm^{-1}): 3426 (m, free water), 3111−3015 (w, sp^2 C−H), 2927 (w, sp^3 C−H), 1656 (s, C=O), 1600 (s, C=N), 1569 (m, C=C), 1459 (s, C=C), 1410 (m, sp^3 methyl C−H bending), 1367 (m), 1082 (w, S=O), 1004 (m, C−O), 963 (m), 908 (s, $[UO_2]_{asymm}$), 850 (w, 1,3-substituted ring sp^2 C−H bend), 842 (w), 778 (m, 1,3-substituted ring sp^2 C−H bend), 704 (w, 1,3-substituted ring sp^2 C−H bend), 679 (w), 645 (w), 575 (w, U−N). These analytical characterization data are in accordance with the prior report of the formation and solid-state structure of **1-UO$_2$** by Rao and co-workers.[15]

1-UO$_2$′. To a refluxing slurry of 2,2′-bipyridyl-6,6′-dicarboxylic acid in methanol (0.049 g, 0.2 mmol) in a 50 mL flask was added triethylamine (0.060 mL, 3 equiv) with stirring in open air, which caused the reaction mixture to become homogeneous. Following this, uranyl acetate dihydrate (0.085 g, 0.2 mmol) in minimal methanol was added, which turned the solution yellow. The solution was allowed to reflux in open air with stirring overnight. The next day, the solution was filtered to remove any trace insoluble material and the filtrate was concentrated *in vacuo* to afford **1-UO$_2$′** as a yellow solid (0.131 g, 99%). ^{1}H NMR (500 MHz, d_4-MeOH) δ (ppm): 9.04 (d, 2H, J = 7.9 Hz), 8.70 (d, 2H, J = 7.6 Hz), 8.62 (t, 2H, J = 7.8 Hz), 3.24 (q, 9H, J = 7.3 Hz), 1.32 (t, 13H, J = 7.2 Hz). ^{13}C{^{1}H} NMR (126 MHz, d_4-MeOH) δ (ppm): 174.37, 158.45, 158.35, 143.81, 128.45, 126.88, 47.87, 9.21. IR spectroscopy (KBr) ν(cm^{-1}): 3426 (m, free water), 3127−3024 (w, sp^2 C−H), 2975 (w), 2938 (w), 2736 (w), 2676 (w), 2492 (w), 1657 (s, C=O), 1601 (m, C=N), 1458 (m, C=C), 1385 (s), 1271 (w, C−N), 1193 (w), 1162 (w), 1035 (w), 1016 (w, C−O), 910 (s, $[UO_2]_{asymm}$), 849 (w, 1,3-substituted ring sp^2 C−H bend), 778 (m, 1,3-substituted ring sp^2 C−H bend), 703 (w, 1,3-substituted ring sp^2 C−H bend), 675 (w), 638 (w), 577 (w, U−N). Anal. Calcd for $C_{18}H_{21}N_3O_6U$ (**1-UO$_2$′**): C 35.35, H 3.45, N 6.85; Found: C 34.97, H 3.41, N 6.13. Calc for $C_{18}H_{21}N_3O_6U$ +

https://doi.org/10.1021/acs.inorgchem.3c02397
Inorg. Chem. 2023, 62, 16131−16148

0.5$(CH_3)_2SO$: C 34.98, H 3.71, N 6.44. This analysis is consistent with the incorporation of 0.5 equiv of DMSO during sample transfer and handling. Single crystals suitable for XRD analysis were obtained by vapor diffusion of diethyl ether into a concentrated solution of the title compound in DMF.

Preparation of 4′-Phenyl-2,2′:6′,2″-terpyridyl-6,6″-dicarboxylic Acid (H_2^{Ph}tdc). The title compound was prepared according to the literature procedure for preparation of closely related **H_2tdc** with relevant modifications.[53] To a solution of 4′-phenyl-2,2′:6′,2″-terpyridyl-6,6″-dicarbonitrile (0.20 g, 0.56 mmol) in 90% ethanol (12 mL) in open air was added a solution of potassium hydroxide (0.33 g, 10.5 equiv) in water (2 mL). The reaction mixture was refluxed with stirring overnight, during which time a white precipitate formed. The next day, the solvent was evaporated *in vacuo* and the resulting solid was suspended in the minimal amount of water. The pH was adjusted to ∼1 with 1 M HCl(aq) and a white solid was collected via vacuum filtration. This solid was then suspended in 1:1 H_2SO_4/CH_3COOH (8 mL total volume) with 4 drops of water and heated at 90 °C for 48 h. The resulting off-white mixture was poured over ice, and a white precipitate formed which was collected via vacuum filtration and washed with water and acetonitrile to give the title compound as an off-white solid (0.22 g, 39%). ^{1}H NMR (400 MHz, d_6-DMSO) δ (ppm): 8.96−8.91 (m, 4H), 8.25 (t, 2H, J = 7.7 Hz), 8.21−8.18 (m, 2H), 7.98 (d, 2H, J = 7.4 Hz), 7.66 (t, 2H, J = 7.4 Hz), 7.59 (dd, 1H, J = 8.4 Hz, J = 6.0 Hz). ^{13}C{^{1}H} NMR (126 MHz, d_6-DMSO) δ (ppm): 165.92, 154.86, 150.15, 148.00, 139.00, 137.53, 129.59, 129.36, 127.24, 125.13, 124.26, 119.20. IR spectroscopy (KBr): ν(cm^{-1}) = 3666-3135 (s, H-bonding with H_2O), 3124−2973 (m, sp^2 C−H stretching), 1733 (s, C=O), 1621 (s, C=N), 1596 (m, C=C), 1584 (m, C=C), 1450 (s, C=C), 1095 (s, C−O), 764 (s, 1,3-substituted ring sp^2 C−H bend), and 695 (m, 1,3-substituted ring sp^2 C−H bend). High Resolution ESI-MS (positive) m/z: expected 420.10; found 420.0968 (H_2^{Ph}tdc + Na$^+$).

Preparation of Ru(^{Ph}tdc)py$_2$ (3-Ru). To a round-bottom flask were added **H_2^{Ph}tdc** (0.075 g, 0.21 mmol), $RuCl_2DMSO_4$ (0.102 g, 0.21 mmol), and methanol (5 mL) in open air. Following degassing with N_2, Hunig's base (0.5 mL, 10 equiv) was added, and the reaction mixture was refluxed with stirring for 24 h, during which time a dark purple precipitate formed. This precipitate was collected via vacuum filtration, redissolved in a mixture of pyridine and water (3:1, total volume 10 mL), degassed under N_2, and refluxed with stirring overnight. The next day, the reaction mixture along with 15 mL of water was placed in a separatory funnel and washed with ethyl acetate (20 mL x 3). The aqueous layer was subjected to vacuum distillation and dried to afford the title compound as a purple solid (0.027 g, 19% yield). See the SI, Figure S8 for the numbering scheme of Ru(^{Ph}tdc)py$_2$. ^{1}H NMR (500 MHz, d_6-DMSO) δ (ppm): 9.13 (s, 2H, *H6*), 8.81 (d, J = 7.9 Hz, 2H, *H9*), 8.31 (d, J = 7.7 Hz, 2H, *H3*), 8.25−8.17 (m, 2H, *H14*), 8.05−7.86 (m, 4H, *H10& H11*), 7.67 (t, J = 7.5 Hz, 2H, *H2*), 7.57 (t, J = 7.6 Hz, 3H, *H1& H16*), 7.10 (t, J = 6.5 Hz, 4H, *H15*). ^{13}C{^{1}H} NMR (126 MHz, d_6-DMSO) δ (ppm): 168.47 (*C13*), 161.74 (*C7*), 158.98 (*C12*), 157.63 (*C8*), 152.59 (*C14*), 142.81 (*C4*), 136.55 (*C16*), 136.30 (*C5*), 135.94 (*C10*), 129.80 (*C1*), 129.22 (*C2*), 127.39 (*C3*), 126.08 (*C11*), 124.59 (*C15*), 123.68 (*C9*), 121.13 (*C6*). Electronic absorption spectrum (DMF): λ_{max} nm (M^{-1} cm^{-1}) = 288 (22,600), 295 (22,600), 338 (19,200), 501 (5,700), 549 (5,000). High Resolution ESI-MS (positive) m/z: expected 678.068; found 678.0648 (Ru(^{Ph}tdc)py$_2$ + Na$^+$). Elemental analysis of **3-Ru** returned unsatisfactory results on multiple occasions; in each case, the C, H, and N contents were significantly below the expected values (see the SI, p. S50 for details). Dark red single crystals suitable for XRD analysis were obtained by the vapor diffusion of diethyl ether into a concentrated solution of the title compound in acetonitrile.

■ ASSOCIATED CONTENT

Supporting Information

The following files are available free of charge. The Supporting Information is available free of charge at https://pubs.acs.org/doi/10.1021/acs.inorgchem.3c02397.

NMR spectra and characterization of complexes; detailed information about X-ray crystallographic data; and Cartesian coordinates of optimized geometries used for computational investigations (PDF)

Cartesian coordinates for structures from XRD (XYZ)

Computational coordinates (XYZ)

Accession Codes

CCDC 2206537−2206538 contain the supplementary crystallographic data for this paper. These data can be obtained free of charge via www.ccdc.cam.ac.uk/data_request/cif, or by emailing data_request@ccdc.cam.ac.uk, or by contacting The Cambridge Crystallographic Data Centre, 12 Union Road, Cambridge CB2 1EZ, UK; fax: +44 1223 336033.

■ AUTHOR INFORMATION

Corresponding Authors

Marco Caricato − *Department of Chemistry, University of Kansas, Lawrence, Kansas 66045, United States;* orcid.org/0000-0001-7830-0562; Email: mcaricato@ku.edu

Chelsea G. Comadoll − *Department of Chemistry, University of Kansas, Lawrence, Kansas 66045, United States; Department of Natural, Health, and Mathematical Sciences, MidAmerica Nazarene University, Olathe, Kansas 66062, United States;* orcid.org/0000-0002-5273-7966; Email: cgcomadoll@mnu.edu

James D. Blakemore − *Department of Chemistry, University of Kansas, Lawrence, Kansas 66045, United States;* orcid.org/0000-0003-4172-7460; Email: blakemore@ku.edu

Authors

Emily R. Mikeska − *Department of Chemistry, University of Kansas, Lawrence, Kansas 66045, United States;* orcid.org/0000-0001-5149-0132

Alexander C. Ervin − *Department of Chemistry, University of Kansas, Lawrence, Kansas 66045, United States*

Kaihua Zhang − *Department of Chemistry, University of Kansas, Lawrence, Kansas 66045, United States*

Gabriel M. Benitez − *Department of Chemistry, University of Kansas, Lawrence, Kansas 66045, United States;* Present Address: Department of Physical and Environmental Sciences, Colorado Mesa University, Grand Junction, Colorado 81501, United States

Samuel M. R. Powell − *Department of Natural, Health, and Mathematical Sciences, MidAmerica Nazarene University, Olathe, Kansas 66062, United States*

Allen G. Oliver − *Department of Chemistry and Biochemistry, University of Notre Dame, Notre Dame, Indiana 46556, United States;* orcid.org/0000-0002-0511-1127

Victor W. Day − *Department of Chemistry, University of Kansas, Lawrence, Kansas 66045, United States*

Complete contact information is available at: https://pubs.acs.org/10.1021/acs.inorgchem.3c02397

Author Contributions

The manuscript was written through contributions of E.R.M., V.W.D., M.C., C.G.C., and J.D.B. All the authors contributed to the design and/or execution of the experimental and computational work reported here. All authors have given approval to the final version of the manuscript.

Notes

The authors declare no competing financial interest.

■ ACKNOWLEDGMENTS

The authors thank the generous faculty of the American Crystallographic Association's Summer Course in Chemical Crystallography for helpful discussions and technical assistance with the structural data reported in this manuscript, Dr. Matthias Zeller (Purdue University) for assistance with refinement of structure a02a, and Dr. Scott Lovell for assistance with diffraction of the data crystal for a02a. The authors also thank Zach Wood and Dr. Megan Fieser (University of Southern California) and Dr. William Brennessel (CENTC Elemental Analysis Facility, University of Rochester funded by NSF CHE-0650456) for assistance with elemental analysis. This work was supported by the U.S. Department of Energy, Office of Science, Office of Basic Energy Sciences through the Early Career Research Program (DE-SC0019169). G.M.B. was supported by NSF REU Program in Chemistry at the University of Kansas (CHE-1950293), and E.R.M. and A.C.E. were supported by a U.S. National Science Foundation Research Traineeship (NRT) at the University of Kansas (DGE-1922649). A preprint reflecting a preliminary version of the findings reported here was posted to a preprint server.[71]

■ REFERENCES

(1) Costa Peluzo, B. M. T.; Kraka, E. Uranium: The Nuclear Fuel Cycle and Beyond. *Int. J. Mol. Sci.* **2022**, *23*, 4655.

(2) *Actinide Separations*; Navratil, J. D.; Schulz, W. W.; American Chemical Society, 1980.

(3) (a) Neidig, M. L.; Clark, D. L.; Martin, R. L. Covalency in f-elements complexes. *Coord. Chem. Rev.* **2013**, *257*, 394−406. (b) Vetteses, G. F.; Morris, K.; Natrajan, L. S.; Shaw, S.; Vitova, T.; Galanzew, J.; Jones, D. L.; Lloyd, J. R. Multiple Lines of Evidence Identify U(V) as a Key Intermediate during U(VI) Reduction by *Shewanella oneidensis* MR1. *Environ. Sci. Technol.* **2020**, *54*, 2268−2276.

(4) (a) Sadergaski, L. R.; Stoxen, W.; Hixon, A. E. Uranyl Peroxide Nanocluster (U_{60}) Persistence and Sorption in the Presence of Hematite. *Environ. Sci. Technol.* **2018**, *52*, 3304−3311. (b) Hua, Y.; Wang, W.; Hu, N.; Gu, T.; Ling, L.; Zhang, W. Enrichment of uranium from wastewater with nanoscale zero-valent iron (nZVI). *Environ. Sci.: Nano* **2021**, *8*, 666−674. (c) You, W.; Peng, W.; Tian, Z.; Zheng, M. Uranium bioremediation with U(VI)-reducing bacteria. *Sci. Total Environ.* **2021**, *798*, No. 149107.

(5) Pattanaude, S. A.; Mullane, K. C.; Schelter, E. J.; Ferrier, M. G.; Stein, B. W.; Bone, S. E.; Lezama Pacheco, J. S.; Kozimor, S. A.; Fanwick, P. E.; Zeller, M.; Bart, S. C. Redox-Active vs Redox-Innocent: A Comparison of Uranium Complexes Containing Diamine Ligands. *Inorg. Chem.* **2018**, *57*, 6530−6539.

(6) Coughlin, E. J.; Qiao, Y.; Lapsheva, E.; Zeller, M.; Schelter, E. J.; Bart, S. C. Uranyl Functionalization Mediated by Redox-Active Ligands: Generation of O−C Bonds via Acylation. *J. Am. Chem. Soc.* **2019**, *141*, 1016−1026.

(7) Spielvogel, K. D.; Couglin, E. J.; Petras, H.; Luna, J. A.; Benson, A.; Donahue, C. M.; Kibasa, A.; Loo, K.; Salacinski, R.; Bart, S. C.; Shaw, S. K.; Shepherd, J. J.; Daly, S. R. The Influence of Redox-Innocent Donor Groups in Tetradentate Ligands Derived from *o*-Phenylenediamine: Electronic Structure Investigations with Nickel. *Inorg. Chem.* **2019**, *58*, 12756−12774.

(8) Fortier, S.; Veleta, J.; Pialat, A.; Le Roy, J.; Ghiassi, K. B.; Olmstead, M. M.; Metta-Magaña, A.; Murugesu, M.; Villagrán, D. $[U(bipy)_4]$: A Mistaken Case of U^0? *Chem. − Eur. J.* **2016**, *22*, 1931−1936.

(9) Natrajan, L.; Burdet, F.; Pécaut, J.; Mazzanti, M. Synthesis and Structure of a Stable Pentavalent-Uranyl Coordination Polymer. *J. Am. Chem. Soc.* **2006**, *128*, 7152−7153.

(10) (a) Selbin, J.; Ortego, J. D. The Chemistry of Uranium(V). *Chem. Rev.* **1969**, *69*, 657−671. (b) Graves, C. R.; Kiplinger, J. L. Pentavalent uranium chemistry − synthetic pursuit of a rare oxidation state. *Chem. Commun.* **2009**, 3831−3853. (c) Arnold, P. L.; Love, J. B.; Patel, D. Pentavalent uranyl complexes. *Coord. Chem. Rev.* **2009**, *253*, 1973−1978.

(11) (a) Arnold, P. L.; Patel, D.; Wilson, C.; Love, J. B. Reduction and selective oxo group silylation of the uranyl dication. *Nature* **2008**, *451*, 315−317. (b) Hayton, T. W.; Wu, G. Exploring the Effects of Reduction or Lewis Acid Coordination on the U = O Bond of the Uranyl Moiety. *Inorg. Chem.* **2009**, *48*, 3065−3072. (c) Schnaars, D. D.; Wu, G.; Hayton, T. W. Reduction of Pentavalent Uranyl to U(IV) Facilitated by Oxo Functionalization. *J. Am. Chem. Soc.* **2009**, *131*, 17532−17533. (d) Schnaars, D. D.; Wu, G.; Hayton, T. W. Borane-Mediated Silylation of a Metal−Oxo Ligand. *Inorg. Chem.* **2011**, *50*, 4695−4697. (e) Cowie, B. E.; Nichol, G. S.; Love, J. B.; Arnold, P. L. Double uranium oxo cations derived from uranyl by borane or silane reduction. *Chem. Commun.* **2018**, *54*, 3839−3842.

(12) Kumar, A.; Lionetti, D.; Day, V. W.; Blakemore, J. D. Redox-Inactive Metal Cations Modulate the Reduction Potential of the Uranyl Ion in Macrocyclic Complexes. *J. Am. Chem. Soc.* **2020**, *142*, 3032−3041.

(13) Faizova, R.; White, S.; Scopelliti, R.; Mazzanti, M. The effect of iron binding on uranyl(V) stability. *Chem. Sci.* **2018**, *9*, 7520−7527.

(14) (a) Hayton, T. W.; Wu, G. Mixed-Ligand Uranyl(V) *β*-Diketiminate/*β*-Diketonate Complexes: Synthesis and Characterization. *Inorg. Chem.* **2008**, *47*, 7415−7423. (b) Nocton, G.; Horeglad, P.; Vetere, V.; Pécaut, J.; Dubois, L.; Maldivi, P.; Edelsein, N. M.; Mazzanti, M. Synthesis, Structure, and Bonding of Stable Complexes of Pentavalent Uranyl. *J. Am. Chem. Soc.* **2010**, *132*, 495−508. (c) Pankhurst, J. R.; Bell, N. L.; Zegke, M.; Platts, L. N.; Lamfsus, C. A.; Maron, L.; Natrajan, L. S.; Sproules, S.; Arnold, P. L.; Love, J. B. Inner-sphere vs. outer-sphere reduction of uranyl supported by a redox-active, donor-expanded dipyrrin. *Chem. Sci.* **2017**, *8*, 108−116. (d) Bell, N. L.; Shaw, B.; Arnold, P. L.; Love, J. B. Uranyl to Uranium(IV) Conversion through Manipulation of Axial and Equatorial Ligands. *J. Am. Chem. Soc.* **2018**, *140*, 3378−3384.

(15) Yang, Y.; Zhang, Z.; Yang, L.; Liu, J.; Xu, C.; Luo, S.; Rao, L. Complexation of U(VI) with BiPDA, DmBiPDA, PhenDA: Comparison on Structures and Binding Strengths in Aqueous and DMSO/20%(v)H_2O Solutions. *Inorg. Chem.* **2019**, *58*, 6064−6074.

(16) Fultz, E. L.; Jones, S. B.; Ivanov, A. S.; Bryantsev, V. S.; Dai, S.; Hancock, R. D. Two Ligands of Interest in Recovering Uranium from the Oceans: The Correct Formation Constants of the Uranyl(VI) Cation with 2,2′-Bipyridyl-6,6′-dicarboxylic Acid and 1,10-Phenanthroline-2,9-dicarboxylic Acid. *Inorg. Chem.* **2022**, *61*, 9960−9967.

(17) Duan, L.; Bozoglian, F.; Mandal, S.; Stewart, B.; Privalov, T.; Llobet, A.; Sun, L. A Molecular Ruthenium Catalyst with Water-Oxidation Activity Comparable to that of Photosystem II. *Nat. Chem.* **2012**, *4*, 418−423.

(18) Nakajima, K.; Toda, H.; Sakata, K.; Nishibayashi, Y. Ruthenium-catalysed Oxidative Conversion of Ammonia into Dinitrogen. *Nat. Chem.* **2019**, *11*, 702−709.

(19) Yazdani, S.; Silva, B. E.; Cao, T. C.; Rheingold, A. L.; Grotjahn, D. B. X-ray crystallography and electrochemistry reveal electronic and steric effects of phosphine and phosphite ligands in complexes of $Ru^{II}(\kappa^4\text{-bda})(PR_3)_2$ and $Ru^{II}(\kappa^3\text{-bda})(PR_3)_3$ (bdc = 2,2′-bipyridine-6,6′-dicarboxylato). *Polyhedron* **2019**, *161*, 63−70.

(20) Donnici, C. L.; Filho, D. H. M.; Moreira, L. L. C.; Teixerira dos Reis, G.; Cordeiro, E. S.; de Oliveira, I. M. F.; Carvalho, S.; Paniago,

https://doi.org/10.1021/acs.inorgchem.3c02397
Inorg. Chem. 2023, 62, 16131−16148

E. B. Synthesis of the Novel 4,4′- and 6,6′- Dihydroxamic - 2,2′-Bipyridines and Improved Routes to 4,4′- and 6,6′- Substituted 2,2′-Bipyridines and Mono-N-Oxide-2,2′-Bipyridine. *J. Braz. Chem. Soc.* **1998**, *9* (5), 455−460.
(21) Fulmer, G. R.; Miller, A. J.; Sherden, N. H.; Gottlieb, H. E.; Nudelman, A.; Stoltz, B. M.; Bercaw, E.; Goldberg, K. I. NMR Chemical Shifts of Trace Impurities: Common Laboratory Solvents, Organics, and Gases in Deuterated Solvents Relevant to the Organometallic Chemist. *Organometallics* **2010**, *29*, 2176−2179.
(22) Sharfalddin, A. A.; Emwas, A.-H.; Jaremko, M.; Hussien, M. A. Complexation of Uranyl (UO_2^{2+}) with Bidentate Ligands: XRD, Spectroscopic, Computational, and Biological Studies. *PloS One* **2021**, *16*, No. e256186.
(23) Because the pentadentate ligands 2,2′:6′,2″-terpyridyl-6,6″-dicarboxylic acid (**H_2tdc**) and 4′-phenyl-2,2′:6′,2″-terpyridyl-6,6″-dicarboxylate (**H_2^{Ph}tdc**) were available from the control work with ruthenium, we also attempted to generate complexes of uranyl with these ligands. Following treatment of **H_2tdc** or **H_2^{Ph}tdc** with NEt_3 in ethanol, the addition of uranyl acetate resulted in immediate precipitation of yellow solids in both cases. We found that these solids (presumed to be uranyl complexes of **tdc** and **^{Ph}tdc**, denoted for reference only as **2-UO_2** and **3-UO_2**, respectively) were insoluble in every solvent available to us, including acetone, DMF, DMSO, and a variety of co-solvent mixtures. Thus, we conclude that forms of **H_2tdc** and **H_2^{Ph}tdc** can react with uranyl acetate, but details regarding the products of this reactivity are not known at this time (see SI, pp. S48 for experimental details).
(24) Duan, L.; Fischer, A.; Xu, Y.; Sun, L. Isolated Seven-Coordinate Ru(IV) Dimer Complex with $[HOHOH]^-$ Bridging Ligand as an Intermediate for Catalytic Water Oxidation. *J. Am. Chem. Soc.* **2009**, *131*, 10397−10399.
(25) Henke, W. C.; Hopkins, J. A.; Anderson, M. L.; Stiel, J. P.; Day, V. W.; Blakemore, J. D. 4,5-Diazafluorene and 9,9′-Dimethyl-4,5-Diazafluorene as Ligands Supporting Redox-Active Mn and Ru Complexes. *Molecules* **2020**, *25*, 3189−3204.
(26) Bard, A. J.; Parsons, R.; Jordan, J. *Standard Potentials in Aqueous Solution*; M. Dekker: New York, 1985.
(27) Sconyers, D. J.; Blakemore, J. D. Electrodeposition behavior of homoleptic transition metal acetonitrile complexes interrogated with piezoelectric gravimetry. *Analyst* **2020**, *145*, 466−477.
(28) Shan, X.; Ibrahim, A. O.; Zhou, Y.; Zhang, H.; Ma, J.; Jiang, F.; Hong, M. Luminescent, second-order NLO and magnetic properties of the hydrogen-bond based network derived from 2,2′-bipyridine-6,6′-dicarboxylate. *Inorg. Chem. Commun.* **2012**, *22*, 149−153.
(29) Gao, Y.; Ding, X.; Liu, J.; Wang, L.; Lu, Z.; Li, L.; Sun, L. Visible Light Driven Water Splitting in a Molecular Device with Unprecedentedly High Photocurrent Density. *J. Am. Chem. Soc.* **2013**, *135*, 4219−4222.
(30) Matheu, R.; Ertem, M. Z.; Benet-Buchholz, J.; Coronado, E.; Batista, V.; Sala, X.; Llobet, A. Intramolecular Proton Transfer Boosts Water Oxidation Catalyzed by a Ru Complex. *J. Am. Chem. Soc.* **2015**, *137*, 10786−10795.
(31) Cowie, B. E.; Purkis, J. M.; Austin, J.; Love, J. B.; Arnold, P. L. Thermal and Photochemical Reduction and Functionalization Chemistry of the Uranyl Dication $[U^{VI}O_2]^{2+}$. *Chem. Rev.* **2019**, *119*, 10595−10637.
(32) Creutz, C. Bipyridine Radical Ions. *Inorg. Chem.* **1982**, *1* (5), 293−311.
(33) Martin, B.; McWhinnie, W. R.; Waind, G. M. 2,2′-Dipyridyl Complexes of Cobalt, Rhodium, and Iridium−II. *J. Inorg. Nucl. Chem.* **1961**, *23*, 207−223.
(34) Hardwick, H. C.; Royal, D. S.; Helliwell, M.; Pope, S. J. A.; Ashton, L.; Goodacre, R.; Sharrad, C. A. Structural, spectroscopic, and redox properties of uranyl complexes with a maleonitrile containing ligand. *Dalton Trans.* **2011**, *40*, 5939−5952.
(35) Burrows, H. D.; Kemp, T. J. The Photochemistry of the Uranyl Ion. *Chem. Soc. Rev.* **1974**, *3*, 139−165.
(36) Syt'ko, V. V.; Umreiko, D. S. Spectroscopic Properties and Electronic Structure of Uranyl Complex Compounds (Review). *J. Appl. Spectrosc.* **1998**, *65*, 857−869.
(37) Hashem, E.; McCabe, T.; Schulzke, C.; Baker, R. Synthesis, structure and photophysical properties of $[UO_2X_2(O = PPh_3]$ (X = Cl, Br, I). *Dalton Trans.* **2014**, *43*, 1125−1131.
(38) Chatelain, L.; White, S.; Scopelliti, R.; Mazzanti, M. Isolation of a Star-Shaped Uranium(V/VI) Cluster from the Anaerobic Photochemical Reduction of Uranyl(VI). *Angew. Chem., Int. Ed.* **2016**, *55*, 14325−14329.
(39) Nockemann, P.; Servaes, K.; Van Deun, R.; Van Hecke, K.; Van Meervelt, L.; Binnemans, K.; Görller-Walrand, C. Speciation of Uranyl Complexes in Ionic Liquids by Optical Spectroscopy. *Inorg. Chem.* **2007**, *146*, 11335−11344.
(40) Bell, J. T.; Biggers, R. E. The Absorption Spectrum of the Uranyl Ion in Perchlorate Media. Part I. Mathematical Resolution of the Overlapping Band Structure and Studies of the Environmental Effects. *J. Mol. Spectrosc.* **1965**, *18*, 247−275.
(41) Smith, N. A.; Cerefice, G. S.; Czerwinski, K. R. Fluorescence and absorbance spectroscopy of the uranyl ion in nitric acid for process monitoring applications. *J. Radioanal. Nucl. Chem.* **2013**, *295*, 1553−1560.
(42) Fortier, S.; Hayton, T. W. Oxo ligand functionalization in the uranyl ion (UO_2^{2+}). *Coord. Chem. Rev.* **2010**, *254*, 197−214.
(43) Redmond, M. P.; Cornet, S. M.; Woodall, S. D.; Whittaker, D.; Collison, D.; Helliwell, M.; Natrajan, L. S. Probing the local coordination environment and nuclearity of uranyl(VI) complexes in non-aqueous media by emission spectroscopy. *Dalton Trans.* **2011**, *40*, 3914−3926.
(44) Connelly, N. G.; Geiger, W. E. Chemical Redox Agents for Organometallic Chemistry. *Chem. Rev.* **1996**, *96*, 877−910.
(45) (a) Cohen, D. The Preparation and Spectrum of Uranium(V) Ions in Aqueous Solutions. *J. Inorg. Nucl. Chem.* **1970**, *32*, 3525−3530. (b) Graves, C. R.; Vaughn, A. E.; Schelter, E. J.; Scott, B. L.; Thompson, J. D.; Morris, D. E.; Kiplinger, J. L. Probing the Chemistry, Electronic Structure and Redox Energetics in Organometallic Pentavalent Uranium Complexes. *Inorg. Chem.* **2008**, *47*, 11879−11891. (c) Bell, N. L.; Shaw, B.; Arnold, P. L.; Love, J. B. Uranyl to Uranium(IV) Conversion through Manipulation of Axial and Equatorial Ligands. *J. Am. Chem. Soc.* **2018**, *140*, 3378−3384. (d) Xin, X.; Douair, I.; Rajeshkumar, T.; Zhao, Y.; Wang, S.; Maron, L.; Zhu, C. Photochemical Synthesis of Transition Metal-Stabilized Uranium(VI) Nitride Complexes. *Nat. Commun.* **2022**, *13*, 3809. (e) Hartline, D. R.; Löffler, S. T.; Fehn, D.; Kasper, J. M.; Heinemann, F. W.; Yang, P.; Batista, E. R.; Meyer, K. Uranium-Mediated Peroxide Activation and a Precursor towards an Elusive Uranium *cis*-Dioxo Fleeting Intermediate. *J. Am. Chem. Soc.* **2023**, *145*, 8927−8938.
(46) Bullock, J. I. Raman and infrared spectroscopic studies of the uranyl ion: the symmetric stretching frequency, force constants, and bond lengths. *J. Chem. Soc. A* **1969**, 781−784.
(47) Henke, W. C.; Stiel, J. P.; Day, V. W.; Blakemore, J. D. Evidence for Charge Delocalization in Diazafluorene Ligands Supporting Low-Valent [Cp*Rh] Complexes. *Chem.—Eur. J.* **2022**, *28*, No. e202200292.
(48) Aspinall, H. C. *f-Block Chemistry*; Oxford University Press: Great Britain, 2020; p 7.
(49) Gore-Randall, E.; Irwin, M.; Denning, M. S.; Goicoechea, J. M. Synthesis and Characterization of Alkali-Metal Salts of 2,2′- and 2,4′-Bipyridyl Radicals and Dianions. *Inorg. Chem.* **2009**, *48*, 8304−8316.
(50) Blakemore, J. D.; Hernandez, E. S.; Sattler, W.; Hunter, B. M.; Henling, L. M.; Brunschwig, B. S.; Gray, H. B. Pentamethylcyclopentadienyl rhodium complexes. *Polyhedron* **2014**, *84*, 14−18.
(51) Andreiadis, E. S.; Demadrille, R.; Imbert, D.; Pécaut, J.; Mazzanti, M. Remarkable Tuning of the Coordination and Photophysical Properties of Lanthanide Ions in a Series of Tetrazole-Based Complexes. *Chem.− Eur. J.* **2009**, *15*, 9458−9476.
(52) Evans, I. P.; Spencer, A.; Wilkinson, G. Dichlorotetrakis-(dimethyl solphoxide)ruthenium(II) and its Use as a Source Material

https://doi.org/10.1021/acs.inorgchem.3c02397
Inorg. Chem. 2023, 62, 16131−16148

for Some New Ruthenium(II) Complexes. *J. Chem. Soc. Dalton.* **1973**, 204−209.
(53) Galaup, C.; Couchet, J.-M.; Bedel, S.; Tisnés, P.; Picard, C. Direct Access to Terpyridine-Containing Polyazamacrocycles as Photosensitizing Ligands for Eu(III) Luminescence in Aqueous Media. *J. Org. Chem.* **2005**, *70*, 2274−2284.
(54) Constable, E. C.; Lewis, J.; Liptrot, M. C.; Raithby, P. R. The Coordination Chemistry of 4′-phenyl-2,2′:6′,2″-terpyridine; the Synthesis, Crystal and Molecular Structures of 4′-Phenyl-2,2′:6′,2″-terpyridine and Bis(4′-phenyl-2,2′:6′,2″-terpyridine)nickel(II) Chloride Decahydrate. *Inorg. Chim. Acta* **1990**, *178*, 47−54.
(55) Mukkala, V.-M.; Helenius, M.; Hemmila, I. Development of Luminescent Europium(III) and Terbium(III) Chelates of 2,2′:6′,2″-terpyridine Derivatives for Protein Labelling. *Helv. Chim. Acta* **1993**, *76*, 1361−1378.
(56) *APEX-4*; Bruker Analytical X-ray Systems Inc.: Madison, WI, USA, 2022.
(57) *SAINT Ver. 8.40A*; Bruker Analytical X-ray Systems Inc.: Madison, WI, USA, 2022.
(58) Krause, L.; Herbst-Irmer, R.; Sheldrick, G. M.; Stalke, D. Comparison of Silver and Molybdenum Microfocus X-ray Sources for Single-Crystal Structure Determination. *J. Appl. Crystallogr.* **2015**, *48*, 3.
(59) Sheldrick, G. M. SHELXT − Integrated Space-Group and Crystal-structure Determination. *Acta Crystallogr., Sect. A: Found. Crystallogr.* **2015**, *A71*, 3−8.
(60) Hübschle, C. B.; Sheldrick, G. M.; Dittrich, B. ShelXle: a Qt Graphical User Interface for SHELXL. *J. Appl. Crystallogr.* **2011**, *44*, 1281−1284.
(61) Frisch, M. J.; Trucks, G. W.; Schlegel, H. B.; Scuseria, G. E.; Robb, M. A.; Cheeseman, J. R.; Scalmani, G.; Barone, V.; Petersson, G. A.; Nakatsuji, H.; Li, X.; Caricato, M.; Marenich, A. V.; Bloino, J.; Janesko, B. G.; Gomperts, R.; Mennucci, B.; Hratchian, H. P.; Ortiz, J. V.; Izmaylov, A. F.; Sonnenberg, J. L.; Williams-Young, D.; Ding, F.; Lipparini, F.; Egidi, F.; Goings, J.; Peng, B.; Petrone, A.; Henderson, T.; Ranasinghe, D.; Zakrzewski, V. G.; Gao, J.; Rega, N.; Zheng, G.; Liang, W.; Hada, M.; Ehara, M.; Toyota, K.; Fukuda, R.; Hasegawa, J.; Ishida, M.; Nakajima, T.; Honda, Y.; Kitao, O.; Nakai, H.; Vreven, T.; Throssell, K.; Montgomery, J. A., Jr.; Peralta, J. E.; Ogliaro, F.; Bearpark, M. J.; Heyd, J. J.; Brothers, E. N.; Kudin, K. N.; Staroverov, V. N.; Keith, T. A.; Kobayashi, R.; Normand, J.; Raghavachari, K.; Rendell, A. P.; Burant, J. C.; Iyengar, S. S.; Tomasi, J.; Cossi, M.; Millam, J. M.; Klene, M.; Adamo, C.; Cammi, R.; Ochterski, J. W.; Martin, R. L.; Morokuma, K.; Farkas, O.; Foresman, J. B.; Fox, D. J. *Gaussian Development Version Revision J.19*; Published online 2020.
(62) Grimme, S.; Anthony, J.; Ehrlich, S.; Krieg, H. A Consistent and Accurate *ab initio* Parametrization of Density Functional Dispersion Correction (DFT-D) for the 94 Elements H-Pu. *J. Chem. Phys.* **2010**, *132*, 154104.
(63) Kulkarni, A. D.; Truhlar, D. G. Performance of Density Functional Theory and Møller−Plesset Second-Order Perterbation Theory for Structural Parameters in Complexes of Ru. *J. Chem. Theory Comput.* **2011**, *7*, 2325−2332.
(64) Andrae, D.; Haeussermann, U.; Dolg, M.; Stoll, H.; Preuss, H. Energy-Adjusted *ab initio* Pseudopotentials for the Second and Third Row Transition Elements. *Theor. Chim. Acta* **1990**, *77*, 123−141.
(65) Rassolov, V. A.; Ratner, M. A.; Pople, J. A.; Redfern, P. C.; Curtiss, L. A. 6-31G* Basis Set for Third-Row Atoms. *J. Comput. Chem.* **2001**, *22*, 976−984.
(66) Lee, C.; Yang, W.; Parr, R. G. Developmeent of the Colle-Salvetti Correlation-Energy Formula into a Functional of the Electron Density. *Phys. Rev. B* **1988**, *37*, 785−789.
(67) Becke, A. D. Density-Functional Thermochemistry. III. The Role of Exact Exchange. *J. Chem. Phys.* **1993**, *98*, 5648−5652.
(68) Cao, X.; Dolg, M. Valence Basis Sets for Relativistic Energy-Consistent Small-Core Lanthanide Pseudopotentials. *J. Chem. Phys.* **2001**, *115*, 7348−7355.
(69) Tarlton, M. L.; Yu, X.; Ward, R. J.; Kelley, S. P.; Autschbach, J.; Walensky, J. R. Backbonding in Thorium(IV) and Uranium(IV) Diarsenido Complexes with tBuNC and CO. *Chem. − Eur. J.* **2021**, *27*, 14396−14400.
(70) Marenich, A. V.; Cramer, C. J.; Truhlar, D. G. Universal Solvation Model Based on Solute Electron Density and on a Continuum Model of the Solvent Defined by the Bulk Dielectric Constant and Atomic Surface Tensions. *J. Phys. Chem. B* **2009**, *113*, 6378−6396.
(71) Mikeska, E. R.; Benitez, G. M.; Zhang, K.; Oliver, A. G.; Caricato, M.; Comadoll, C. G.; Blakemore, J. D. Evidence for Ligand- and Metal-Centered Reduction in Polypyridyl Dicarboxylate Complexes of Ru(II) and U(VI). *ChemRxiv (Inorg. Chem.)* **2022**, DOI: 10.26434/chemrxiv-2022-jbc9n.

https://doi.org/10.1021/acs.inorgchem.3c02397
Inorg. Chem. 2023, 62, 16131−16148